Stochastic in Space and Time: Part 2, Effects of Simulating Orographic Gradients in Daily Runoff Variability on Bedrock River Incision

A.M. Forte[1] and M.W. Rossi[2]

[1] Department of Geology and Geophysics, Louisiana State University, Baton Rouge, Louisiana, USA.
[2] Earth Lab, Cooperative Institute for Research in Environmental Sciences (CIRES), University of Colorado, Boulder, Colorado, USA.

Corresponding author: Adam M. Forte (aforte8@lsu.edu)

Key Points:

- Relationships between runoff, runoff variability, and topography in mountainous terrain can explain pseudo-thresholds in channel steepness
- Extent to which exceedance frequency of runoff generating events is spatially coherent is an unrecognized control on landscape evolution
- Orographic patterns in variability, snowmelt, and characteristic size of runoff events crucial for progress on climate-tectonic coupling

Abstract

Understanding the extent to which climate and tectonics can be coupled requires knowing both the form of topography and erosion rate relationships, but also the underlying mechanistic controls on those forms. The stream power incision model (SPIM) is commonly used to interpret such topography erosion rate relationships, but is limited in terms of probing mechanisms. A promising modification is a stochastic-threshold incision model (STIM) which incorporates both variability in discharge and a threshold to erosion, and in which the form of the topography erosion rate relationship is largely controlled by the variability of runoff. However, as applied STIM assumes temporally variable, but spatially constant runoff generating events, an assumption that is likely broken in regions with complicated orography. In response, we develop a unique 1D STIM based profile model that allows for stochasticity in both time and space and is driven by empirical relations between topography and runoff statistics. Testing the development of steady-state topography using spatial-STIM over a range of uplift rates highlights that coupling between mean runoff, runoff variability, and topography suggest that the development of highly nonlinear topography erosion rates should be expected. Further, we find that whether the daily statistics of runoff generating events are spatially linked or unlinked is a primary control on landscape evolution and the final resulting topography. As many empirical topography – erosion rate datasets likely sample across ranges of linked vs unlinked behavior, it is questionable whether single SPIM relationships fit to those data, without considerations of the hydroclimatology, are meaningful.

Plain Language Summary

A long-standing question in tectonics is whether spatial patterns in precipitation resulting from growing mountains in turn influence internal deformation of those ranges. Critical to this is how topography, as the interface between surface and tectonic processes, responds to changes in rock uplift rate as this sets the "sensitivity" of the landscape and controls the strengths of feedbacks. Prior work suggests variability of daily runoff is an important control on this sensitivity, with low variability regions expected to have low sensitivity and thus a reduced capacity for climate-tectonic coupling. Critically, much of this prior work considers runoff that is variable in time, but not space, which does not necessarily honor observations of complex precipitation patterns in mountains. Here we develop a simple numerical model, built using observed relationships between runoff, runoff variability, and topography, to test this and find that the degree to which runoff events are linked or unlinked in space is actually an important control on both the sensitivity of landscapes but also the total relief of those landscapes. Our results suggest that consideration of the size of runoff generating events within landscapes is an ignored control on topography, but fundamental for progress on questions of climate-tectonic coupling.

1 Introduction

1.1. Motivation

The potential for two-way coupling between climate and tectonics is premised on how climate, erosion, and topography are related. Stream power provides an effective way to model the role of climate on erosion via a single parameter, the erodibility coefficient (Howard, 1994; Whipple & Tucker, 1999). When stream power is used as the principal erosion law, landscape evolution studies predict that climate should strongly influence the pattern and style of deformation in mountain belts (Beaumont et al., 1992; Whipple & Meade, 2006; Willett, 1999). These numerical models show how prevailing wind direction, along with an orographic enhancement of precipitation, leads to across-strike asymmetry in the efficiency of erosion of the landscape. However, field verification of such dynamics has been elusive, with ambiguous evidence both for and against coupling between mean precipitation and tectonics (see discussion in Whipple, 2009). One barrier to field verification is uncertainty in how well suited stream power predictions are for isolating relationships among climate, erosion, and bedrock river morphology. Given the proliferation of carefully curated datasets attempting to constrain how climate is embedded in the erodibility coefficient (e.g., Adams et al., 2020; Ferrier et al., 2013; Forte et al., 2022; Leonard et al., 2023), the time is ripe to re-visit assumptions implied by conventional applications of stream power to landscape evolution studies, especially in the context of the complexities that result from orographic precipitation (e.g., Anders et al., 2006, 2007; Bookhagen & Burbank, 2006; Bookhagen & Strecker, 2008; Roe, 2005; Roe et al., 2003).

Since development of these early landscape evolution models, a large body of work has refined our understanding of the strengths and limitations of stream power (see summary in Lague, 2014). We highlight three sets of insights: (1) Probabilistic assessment of floods are needed when erosional thresholds matter (Lague et al., 2005; Snyder et al., 2003; Tucker, 2004); (2) Orographic gradients in mean precipitation lead to spatially non-uniform patterns in runoff generation (Bookhagen & Strecker, 2008; Roe et al., 2002, 2003); and (3) Precipitation phase (i.e., rain versus snow) mediates spatio-temporal patterns in runoff generation (Anders et al., 2008; Bookhagen & Burbank, 2010; Rossi et al., 2020). While there are a number of important limitations to using stream power (e.g., channel width scaling, tools-cover effects), we focus here on those related to the ‘characteristic discharge’ assumption typically used in stream power. Our work builds on recent studies that show how daily runoff variability sets the nonlinearity between equilibrium channel steepness with long term erosion rates (Campforts et al., 2020; Desormeaux et al., 2022; Forte et al., 2022; Marder & Gallen, 2023). In stream power predictions that use the characteristic discharge assumption, nonlinear relationships are interpreted to reflect differences in the incision process setting the slope exponent, n. However, if erosional thresholds matter, nonlinearity is instead linked to the variability of streamflow (see discussion in Lague, 2014). Given the wide range of empirical estimates for n reported in the literature (Harel et al., 2016), we argue that river incision models likely require more hydrologic realism to explain observed nonlinearities between channel steepness and erosion rate (e.g., Deal et al., 2018).

1.2. Approach and Scope

The basis for our work is the stochastic-threshold incision model (STIM) proposed by Lague et al. (2005), albeit a modified version whereby daily discharge distributions are treated as Weibull distributions instead of inverse gamma distributions (following Forte et al., 2022). As originally conceived, this 1D river incision model uses the shear stress formulation of stream power as the instantaneous incision law. The equilibrium longitudinal profile for a given rate of base level fall is then derived by integrating the product of the instantaneous incision law and the probability distribution of flows, with a lower bound of integration set by the erosion threshold. While there are many hard-to-constrain parameters in STIM, this model improves on the stream power incision model (SPIM) by explicitly showing how two hydroclimatic parameters, the mean runoff and a shape parameter describing the distribution of runoff events, alter the form of the relationship between long-term denudation rates and channel steepness (DiBiase & Whipple, 2011; Lague et al., 2005). A key assumption in STIM is that runoff generating events are stochastic in time but not in space. For small catchments with relatively uniform surface properties, this is a reasonable assumption. However, as the size of watersheds increases and as surface properties become more heterogeneous, the potential importance of partial source areas for runoff generation during events are expected to become more important (Dunne & Black, 1970). This is likely exacerbated in high-relief landscapes where complicated orography leads to significant spatial and temporal variation in precipitation (e.g., Anders et al., 2006, 2007; Barros et al., 2000; Campbell & Steenburgh, 2014; Frei & Schär, 1998; Minder et al., 2008) and thus potentially runoff. It is however not our intention to embed a full hydrological model of event-scale runoff generation into a 1-D model of river incision. Instead, we seek to add flexibility to STIM such that we can explore how runoff statistics that vary in *both* space and time alter model predictions.

There are four key novelties to our new1D stochastic-threshold model of bedrock incision, which we refer to as spatial-STIM. First, the longitudinal profile is subdivided into uniform bins that allow us to evolve orographic gradients in hydroclimate. Second, both mean runoff and daily runoff variability are dictated by their relationship to topography, i.e., local relief, elevation. Third, these topography-hydrology relationships are based on relationships observed in modern mountain landscapes developed in our companion manuscript to this one (Forte & Rossi, In Review) and explicitly consider the role of snowmelt in modulating runoff variability. Fourth, the temporal stochasticity of each bin can either be 'linked' or 'unlinked' spatially. This allows for examination into how the characteristic spatial scale of runoff events will impact model predictions. We focus our analysis of model sensitivity to the new elements introduced in spatial-STIM, the orographic rules used to set streamflow parameters, and changes in rock uplift rates. As such, our results are not intended to provide formal model calibration and validation using erosion rate data. Instead, our goal is to show how spatial-STIM might alter interpretations of the numerous channel steepness-erosion rate relationships reported in the literature and to probe general expectations of how such relationships might evolve as a mountain range grows (Figure 1).

Our conceptual framework builds on the findings from the companion manuscript to this one (Forte & Rossi, In Review). The central hypothesis underlying our modeling derives from observations that both mean runoff and snowmelt fraction are functionally related to topography (Figure 1A). Increases in both are tied to decreasing variability in daily streamflow (Figure 1B), which itself causes increasingly nonlinear relationships between channel steepness and erosion rates (Figure 1C). As suggested by Forte et al., (2022), this set of expected relationships predicts a somewhat neglected negative orographic feedback in which the continued topographic growth of a mountain range may be fundamentally limited by the decreasing variability of streamflow and increasing nonlinearity in topography and channel steepness relationships (Figure 1). A fundamental question then is whether such relationships will develop when runoff, runoff variability, and snowmelt are all coupled to topography. We address this question by developing spatial-STIM and conducting a suite of numerical experiments presented below.

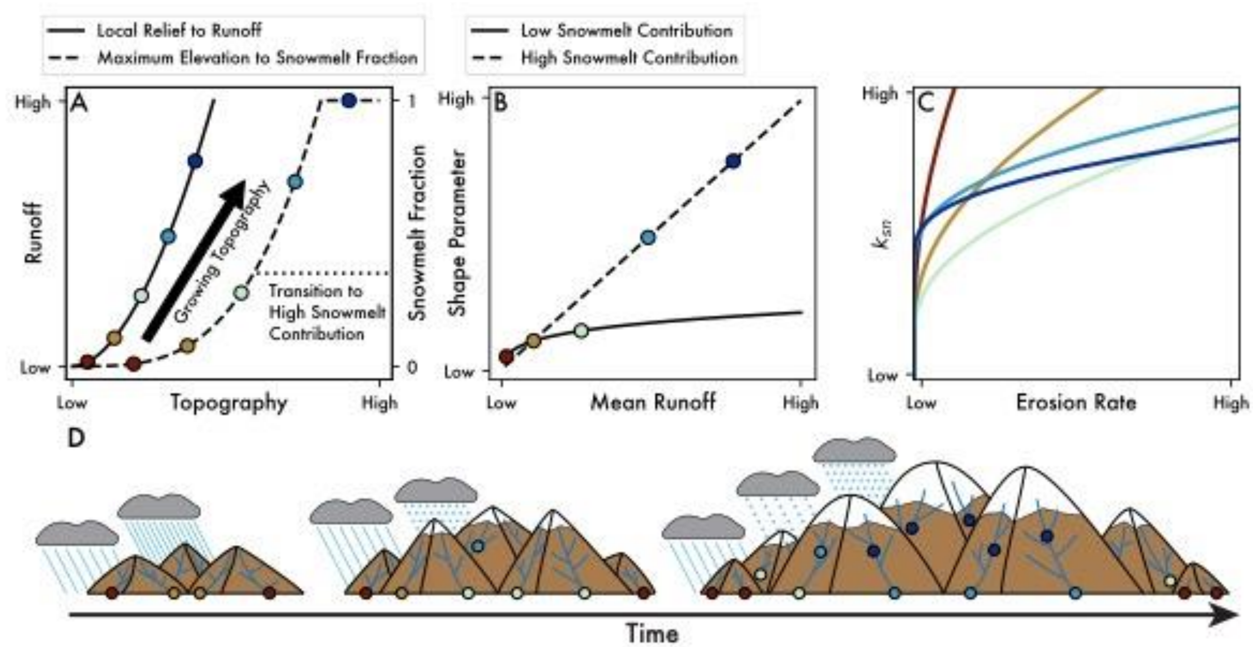

Figure 1. Conceptual model of how covariation of topography, mean runoff, snowmelt fraction of runoff, and runoff variability influences the ksn-E relationships as topography grows. A) Relationships between local relief and mean runoff (solid line) and maximum elevation and the fraction of runoff derived from snowmelt (dashed line). Horizontal dotted line indicates snowmelt fraction where runoff-variability relationships transition from a power law to a linear form. Colored dots represent hypothetical states as topography grows. B) Relationship between mean runoff and variability. Solid line is a power law relationship that characterizes conditions when snowmelt contribution is limited. Dashed line is a linear relationship that characterizes conditions when snowmelt contribution is significant. C) Implied ksn-E relationships for the different mean runoff - variability relationship from B. D) Schematic envisioning how the relationships in A-C might evolve through time and space as a mountain range grows. The colored dots are meant to suggest that portions of streams above those dots would be dictated by the relationships of the respective color in A-C.

2. Background

2.1. Channel Steepness and Erosion Rate Relationships

For river analysis, it is useful to define a channel steepness index (k_s) that accounts for the expected covariation of slope and drainage area within river systems (Flint, 1974):

$$k_s = A^{\theta} S \tag{1}$$

where A is drainage area [L^2], S is local river slope [L/L], and θ is a dimensionless constant that describes the concavity of the river profile. In order to compare channel steepnesses for rivers with different concavities, the steepness index k_s can be normalized by setting θ to a reference value, θ_{ref}, thereby defining a normalized channel steepness index, k_{sn} (Wobus et al., 2006). Normalized channel steepness can be determined via regression of the log-transformed, slope-area data along river profiles (Kirby & Whipple, 2012). However, it is now more common to use the so-called χ-transform to calculate k_{sn} because of the noise inherent in slope-area data (Whipple et al., 2022). As defined by Perron & Royden (2013), χ is an integral transform of distance such that:

$$\chi = \int_{x_b}^{x} (A_0/A(x))^{\theta_{ref}} dx \tag{2}$$

where A_0 is a reference drainage area, x is distance from the catchment outlet, and x_b is the position of the outlet. On a plot of χ-elevation, an equilibrium channel with a uniform k_{sn} appears as a straight line, assuming an appropriate θ_{ref} is used in the calculation of χ. When A_0 is set to one, the slope of the χ-elevation line equals k_{sn}.

Relationships between catchment averaged normalized channel steepness and long-term erosion rates, E, show that: (1) k_{sn} tends to be positively correlated with average erosion rate, but that (2) the exact form of k_{sn}-E relationships varies substantially among landscapes (see compilations in Harel et al., 2016; Kirby & Whipple, 2012; Lague, 2014; Marder & Gallen, 2023). The general form of these relationships follow:

$$k_{sn} = CE^{\Phi} \tag{3}$$

where C and Φ are constants that vary between locations. To interpret these empirical relationships, it is common to recast Equation 3 in terms of a widely used model for fluvial incision into bedrock, the stream power incision model (SPIM, Howard, 1994; Whipple & Tucker, 1999). SPIM considers erosion in terms of an erosional efficiency parameter (K) that encapsulates aspects of both climate and lithology, along with A and S:

$$E = KA^m S^n \tag{4}$$

where m and n are both constants thought to represent details of the hydrology and erosional process, respectively. In Equation 4, A is a proxy for mean discharge $\bar{Q}$ [L^3/t] and implicitly assumes a simple relationship between mean discharge, mean runoff $\bar{R}$ [L/t], and drainage area such that $\bar{Q} = \bar{R}A$. The erosional efficiency parameter, K, embeds $\bar{R}^m$ thereby directly relating K to the hydroclimatology. By combining Equations 1, 3, and 4 in SPIM, it can be readily shown that:

$$\theta = \frac{m}{n}, \tag{5}$$

$$C = K^{-1/n}, \tag{6}$$

$$\Phi = \frac{1}{n}, \tag{7}$$

and thus,

$$k_{sn} = K^{-1/n} E^{1/n} \text{ or } E = K k_{sn}^n \tag{8}$$

Equation 8 predicts that the form of the k_{sn}-E relationship can be cast in terms of variations in climate and lithology (represented by K) and erosional process (represented by n). Implicit in this relationship is also the assumption that the basin-averaged value of k_{sn} and E are steady state values, i.e., erosion rate approximately equals long-term rock uplift rate and that the k_{sn} within the watershed in question is spatially uniform and free of transients, e.g., knickpoints.

Recently, it has been shown that relationships between channel steepness and erosion rates can be further interrogated by disentangling the climate and lithologic components of the erosional efficiency parameter, K, by defining an alternate form of k_{sn} that includes a proxy for discharge. This new index, k_{snQ}, was defined by Adams et al., (2020):

$$k_{snQ} = \bar{Q}^{\theta_{ref}} S. \tag{9}$$

Calculations of k_{snQ} typically use mean precipitation as a proxy for mean runoff to calculate discharge, embedding a simplifying assumption that mean runoff will linearly scale with mean precipitation. Using the same assumption in Equation 3 that $\bar{Q} = \bar{R}A$, it is possible to recast K as:

$$K = K_{lp}\bar{R}^{m} \tag{10}$$

where K_{lp} is the component of the erosional efficiency related to lithology and associated details such as sediment flux dynamics and erosion thresholds. The relationship between k_{sn}-E in Equation 8 can then be reformulated as:

$$k_{snQ} = K_{lp}^{-1/n} E^{1/n} \text{ or } E = K_{lp} k_{snQ}^{n} \tag{11}$$

This alternative formulation of channel steepness acknowledges spatially varying precipitation and runoff and thus should reduce the role of climate in the topography – erosion rate relationship, allowing both more accurate use of topography to estimate erosion rates (Adams et al., 2020) and isolation of lithologic controls on erosion rate (Leonard et al., 2023).

Importantly, interpretation of either k_{sn}-E and k_{snQ}-E relationships within a SPIM framework relies on a similar set of simplifying assumptions that have been articulated in more detail elsewhere (e.g., Harel et al., 2016; Kirby & Whipple, 2012; Lague, 2014). However, we highlight here one important implication of SPIM to how the slope exponent in stream power, n, and the empirical exponent, Φ, are interpreted. Considering a steady state system where erosion rates balance uplift rates, the value of n controls the degree of nonlinearity, Φ (Eq. 7). When $n \approx 1$, this defines a linear relationship between topography and erosion rate and implies that rivers maintain a uniform sensitivity to changes in rock uplift rate as they steepen. In contrast, when $n \gg 1$, and when E is plotted on the abscissa, the strongly sublinear relationship between topography and erosion rate implies that channel steepness reaches a pseudo-threshold as uplift rates continue to increase. Higher values of n lead to a reduced potential for two-way coupling between climate and tectonics as topography is no longer able to adjust to increases in rock uplift rates (Whipple & Meade, 2004). Global compilations of k_{sn}-E suggest that $n \approx 2$ (e.g., Harel et al., 2016; Lague, 2014), implying a sublinear response, but not one where significant pseudo-thresholds in k_{sn} limits the relief of mountain landscapes (Hilley et al., 2019). However, at the individual landscape scale, substantial difference in values of n are observed, with some locations suggesting more linear relationships (e.g., Ferrier et al., 2013; Safran et al., 2005; Wobus et al., 2006), while others exhibit highly sublinear relationships that imply pseudo-thresholds in k_{sn} (e.g., Cyr et al., 2010; Forte et al., 2022; Hilley et al., 2019). However, diagnosing the underlying mechanisms for these large differences is limited by relying on stream power alone.

2.2. Stochastic-Threshold Incision Model (STIM)

To probe controls on the nonlinear k_{sn}-E relationships described above, we show that it can be useful to consider an alternative fluvial incision model, specifically the stochastic-threshold incision model (STIM). STIM shares some similarities with SPIM, but adds two important details, (1) discharge varies in time and (2) not all discharges are able to erode. Different formulations of stochastic-threshold incision models have been presented (e.g., Snyder et al., 2003; Tucker, 2004), but here we primarily focus on the version presented by Lague et al., (2005). The details of this model have been discussed in depth previously (e.g., Campforts et al., 2020; DiBiase & Whipple, 2011; Lague et al., 2005; Scherler et al., 2017) to which we refer interested readers. Here we briefly present the governing equations, focusing on differences from the original formulation of Lague et al., (2005).

STIM uses an equation for instantaneous (e.g., daily) incision rates and then integrates this over a probability distribution of daily discharges to calculate the average, long-term erosion rate. In the original formulation by Lague et al., (2005), both the instantaneous incision and average erosion rates were cast in terms of dimensionless discharge. Because we are breaking the assumption of $\bar{Q} = \bar{R}A$, it is more useful to define the instantaneous law in terms of dimensional runoff (*R*):

$$I = K k_{sn}^{n} \bar{R}^{m-\gamma} R^{\gamma} - \Psi_c \tag{12}$$

where γ is an exponent describing local discharge and Ψ_c is the threshold parameter. Functionally, *K*, *m*, and *n* are similar to their counterparts in Equation 3, but have more formal definitions such that

$$K = k_e k_t^{a} k_w^{-a\alpha} \tag{13}$$

$$m = a\alpha(1 - \omega_a) \tag{14}$$

$$n = a\beta \tag{15}$$

where k_e is a rock erodibility coefficient, k_t, α, and β are hydraulic and frictional constants, k_w and ω_a are constants related to channel width scaling with discharge, and *a* is an constant related to incisional process. The threshold parameter Ψ_c is related to both the rock erodibility and incisional process such that

$$\Psi_c = k_e \tau_c^{a} \tag{16}$$

where τ_c is the critical shear stress for initiatining incision. To calculate an average, steady state erosion rate *E*, Equation 12 must be integrated across a range of runoffs

$$E = \int_{R_c(k_{sn})}^{R_m} I(R, k_{sn}) pdf(R) dR \tag{17}$$

where R_c is the critical runoff for overcoming the incision threshold, R_m is an arbitrarily high upper bound on runoff assuming that the integral is convergent, and *pdf(R)* is the probability distribution of daily runoff. In the original formulation of Lague et al., (2005), the probability distribution function used was the inverse gamma distribution of normalized discharge, thus fixing the scale parameter to 1. Here, we follow recent work (Forte et al., 2022; Rossi et al., 2016) by using a two component Weibull distribution on non-normalized runoff

$$pdf(R; R_0, c_R) = \frac{c_R}{R_0}\left(\frac{R}{R_0}\right)^{c_R - 1} exp^{-1(R/R_0)^{c_R}} \tag{18}$$

where R_0 is a scale parameter, related to the mean of the distribution, and c_R is a shape parameter, describing the variability of daily flows. Higher values of c_R imply lower variability.

With respect to k_{sn}-E patterns, Lague et al., (2005) highlight that the degree of linearity of such relationships in the context of STIM is largely controlled by daily runoff variability, or the shape parameter of the runoff distribution in the domain where the erosion thresholds are large with respect to the erosion rates (Regime III in Lague et al., 2005). While Lague et al., (2005) used an inverse gamma distribution to make this case, Rossi et al., (2016) showed empirically that the shape parameters of distributions fit with inverse gamma and a Weibull distribution are linearly related. The Weibull distribution can thus be confidently substituted into Equation 17, with the basic effect of moderating the impact of heavy tailed distributions produced using the inverse gamma distribution for some values of the shape parameter. Regardless of distribution choice, STIM predicts that low variability systems should exhibit sublinear k_{sn}-E relationships, whereas highly variable systems will be characterized by more linear k_{sn}-E relationhips. Thus, one explanation of the wide range of empirical values for Φ might be due to landscape-scale differences in daily runoff variability (Marder & Gallen, 2023).

3 Orographic Relationships Between Hydroclimatology and Topography

In the companion manuscript to this one (Forte & Rossi, In Review), we use a 20 year global, daily time series of hydroclimate from the Water Global Assessment and Prognosis (WaterGAP3 - Alcamo et al., 2003; Döll et al., 2003) along with the HydroSheds v1, 15 arcsecond digital elevation model (Lehner et al., 2008) and SRTM-90 data (Farr et al., 2007) to develop a variety of empirical relationships between hydroclimatological and topographic variables. We refer interested readers to Forte & Rossi (In Review) for more detailed discussions, but review the primary results of this analysis here that form the basis for the empirical relationships we implement in our 1D spatial-STIM model as summarized in Figure 2.

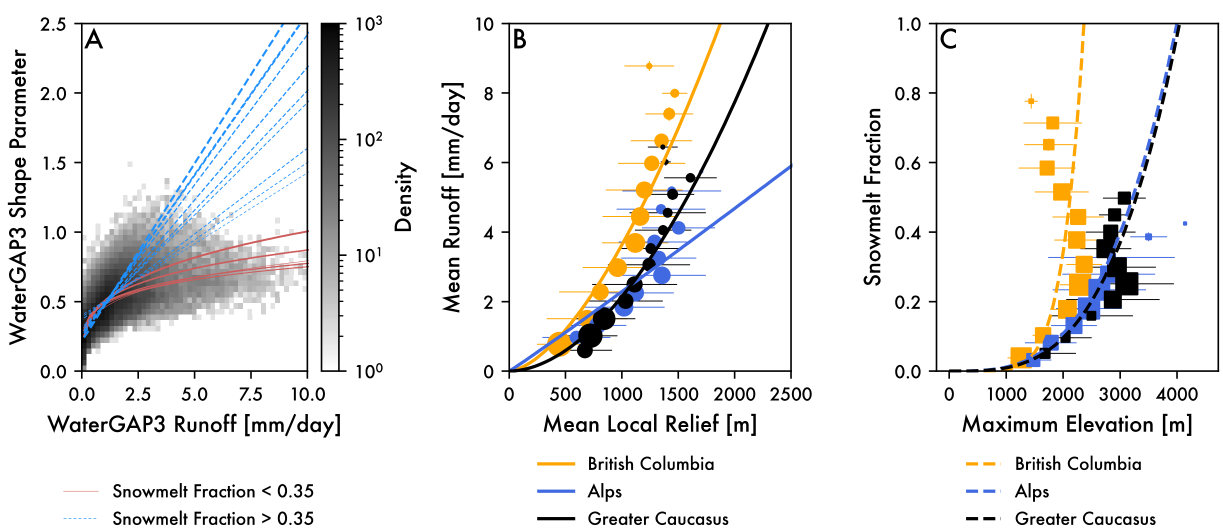

Figure 2. Summary of empirical results from Forte & Rossi (In Review) used relate topography and hydroclimatological variables of interest. A) Relationship between mean daily runoff ($\bar{R}$) and daily runoff variability as parameterized by the Weibull shape parameter (c_R). Colored lines indicate individual fits to $\bar{R}$ and c_R values within bins defined by snowmelt fraction (SF). Red solid lines are power law fit for bins with SF < 0.35 and blue dashed lines are linear fits for bins

with SF > 0.35. B) Power law fits between mean local relief and $\bar{R}$ for the three exemplar regions. C) Power law fits between maximum elevation and SF for the three exemplar regions.

Specifically, Forte & Rossi (In Review) find a similar inverse correlation between $\bar{R}$ and variability (Figure 2A) as has been identified in smaller datasets from gauged watersheds (e.g., Molnar et al., 2006; Rossi et al., 2016). Similar to Rossi et al., (2016), they note that the form of this relationship between $\bar{R}$ and variability, as parameterized by c_R (Eq. 18) is controlled by the relative contribution of snowmelt to total runoff, which they characterize with the parameter *SF* where *SF* is equal to the total amount of runoff from snowmelt divided by the total runoff. When *SF* is low and snowmelt is not dominant, the relationship between $\bar{R}$ and c_R takes the form of a power law, but when *SF* is high, this relationship instead is linear (Figure 2A). In the WaterGAP3 data, this change from power law to linear behavior occurs at a *SF* of ~0.35.

In the context of parameterizing our 1D STIM model, where we wish to evolve these parameters as a function of topographic growth, it follows that to uniquely prescribe the distribution of flows (e.g., Equation 18) within a part of a river profile, we need to know both $\bar{R}$ and *SF* to then uniquely identify an appropriate c_R. As described in Forte & Rossi (In Review), identifying singular relationships between either $\bar{R}$ or *SF* and topographic metrics proves challenging due to a variety of regional variations. Instead, we use the three representative example regional relationships Forte & Rossi (In Review) develop between mean local relief and $\bar{R}$ and maximum elevation and *SF* in the Greater Caucasus, European Alps, and northern British Columbia (Figure 2B-C). For all three locations and both relationships, a power law provided the best fit relationship between the variables.

Local relief and local maximum elevation (e.g., within a WaterGAP3 pixel) are not typically explicit to models of river profile development because they represent the interaction between fluvial and hillslope processes. While these topographic metrics are thought to be linked to river morphology at certain spatial scales, how to best use these scale-dependent metrics to drive rules in a 1D river incision model is not entirely obvious. Given our discretization of river profiles into bins, we argue there is a sensible way to honor the empirical relationships we show in Figure 2 into a 1D river incision model. For example, it has been shown that local relief at the 2 to 2.5 km radius scale is linearly correlated with channel steepness (e.g., DiBiase et al., 2010). Channel steepness is a property of the river profile that can be calculated (Equation 1) and updated as the river profile evolves through time. Based on this, we constrain how local relief is related to channel steepness in our three selected regions by building on the methods described in Forte et al., (2016), using a combination of TopoToolbox (Schwanghart & Scherler, 2014) and the Topographic Analysis Kit (Forte & Whipple, 2019). First, we extract all watersheds with a drainage area >50 km^2 and an outlet above 300 m elevation. Any watershed from this initial extraction with a drainage area >250 km^2 was then subdivided into tributary watersheds that connect to the trunk channel using drainage areas >50 km^2 as a threshold. For each catchment at a site, mean channel steepness and local relief (2500 m radius) was calculated along with the R^2 value for a linear fit between χ (Equation 2) and elevation. Values of R^2 close to 1 imply a river reach that is largely free of major knickpoints. The R^2 values were thus used to screen for reaches in quasi-equilibrium such that only reaches above a high threshold (>0.95; Figure S1) were used to develop regionally based relationships between channel steepness and local relief. By establishing the channel steepness to local relief relationship for each site, we can then apply empirically based, hydroclimatological rules based on local relief into our river incision model. As channel steepness evolves in our model, it is directly tied to local relief and indirectly tied to maximum elevation by adding the appropriate local relief to the minimum elevation of the profile for a given bin.

4 River Incision Model

While there are now many studies testing the utility of the 1D Stochastic-Threshold Incision Model (STIM) developed by Lague et al. (2005) (e.g., Campforts et al., 2020; Desormeaux et al., 2022; DiBiase & Whipple, 2011; Forte et al., 2022; Marder & Gallen, 2023; Scherler et al., 2017), we believe this paper is the first attempt to modify a 1D version of STIM to allow for stochastic events in space as well as time, which we refer to as spatial-STIM. Our modelling strategy shares some similarity with recent 2D efforts to consider the role of spatial variability in precipitation events (e.g., Coulthard & Skinner, 2016; Peleg et al., 2021), but these efforts considered landscape evolution at timescales orders of magnitude shorter than we do here. By subdividing the long profile into bins we can coevolve the hydrology with the local channel morphology. However, binning alone only entails flexibility to vary the magnitude of stochastic runoff for a given bin. A decision needs to be made for whether spatial bins should depend on each other (i.e., runoff events are synchronous across the profile) or be treated independently (e.g., bins experience different storms or snowmelt events). We refer to the former as the 'linked' case and the latter as the 'unlinked' one. Once we chose the model scenarios, we test the sensitivity of model outputs to the model setup and hydroclimatic rules developed for the three regional cases.

4.1. Spatial-STIM

Our 1D bedrock incision model was developed in Python 3.10 by implementing an explicit upwind finite difference solution of Equation (12) for instantaneous incision along the profile. In keeping with the underlying assumptions of STIM, all models are run at a daily timestep. The starting condition for each model uses a drainage area distribution based on the relationship between profile length (L) [L] and drainage area (A) [L^2] from Sassolas-Serrayet (2018):

$$L = cG_cA^{n_A} \tag{19}$$

$$c = 0.5G_c\sqrt{\pi} + 0.25\sqrt{{G_c}^2\pi - 4} \tag{20}$$

where G_c, or the Gravelius coefficient, is set to 1.5 and the exponent n_A is set to 0.54. This form of the relationship between drainage area and stream distance is useful because it allows for direct consideration of the shape of the drainage basin using a single parameter. A watershed with a G_c of 1 has a perfectly circular boundary and a watershed with a G_c of 2 is an narrow, elongated watershed. Because we are only simulating the river profile, we use a threshold drainage area, A_c, of 1 km^2. Using the specified G_c and n_A from above, this is equivalent to the Hack (1957) relationship of the form:

$$A = k_aL^h + A_c \tag{21}$$

where k_a = 0.969 and h =1.851. For all runs, we set the spacing between nodes at 100 meters and saved outputs every 5000 years. All runs are initialized with a starting profile with a low and constant k_{sn} of 25 m.

Spatial variations in both mean runoff and runoff variability, i.e., shape parameter, are handled by adopting uniform river length bins along the longitudinal profile. Each bin has a single scale and shape parameter for all the nodes within the bin. At each time step, these parameters are recalculated based on the current topography. Figure 3 shows an example for how the mean runoff and shape parameter vary as a function of bin location at one time step during a transient. The location and dimensions of bins are fixed for each model run to maintain computational efficiency. However, our analysis of model sensitivity includes varying the bin size and number of bins within a profile to test the sensitivity of the results to these choices (see section 5.4). The key property of our model that allows hydroclimatology to coevolve with the topography occurs in the method we use to the recalculate the shape and scale parameters at every time step.

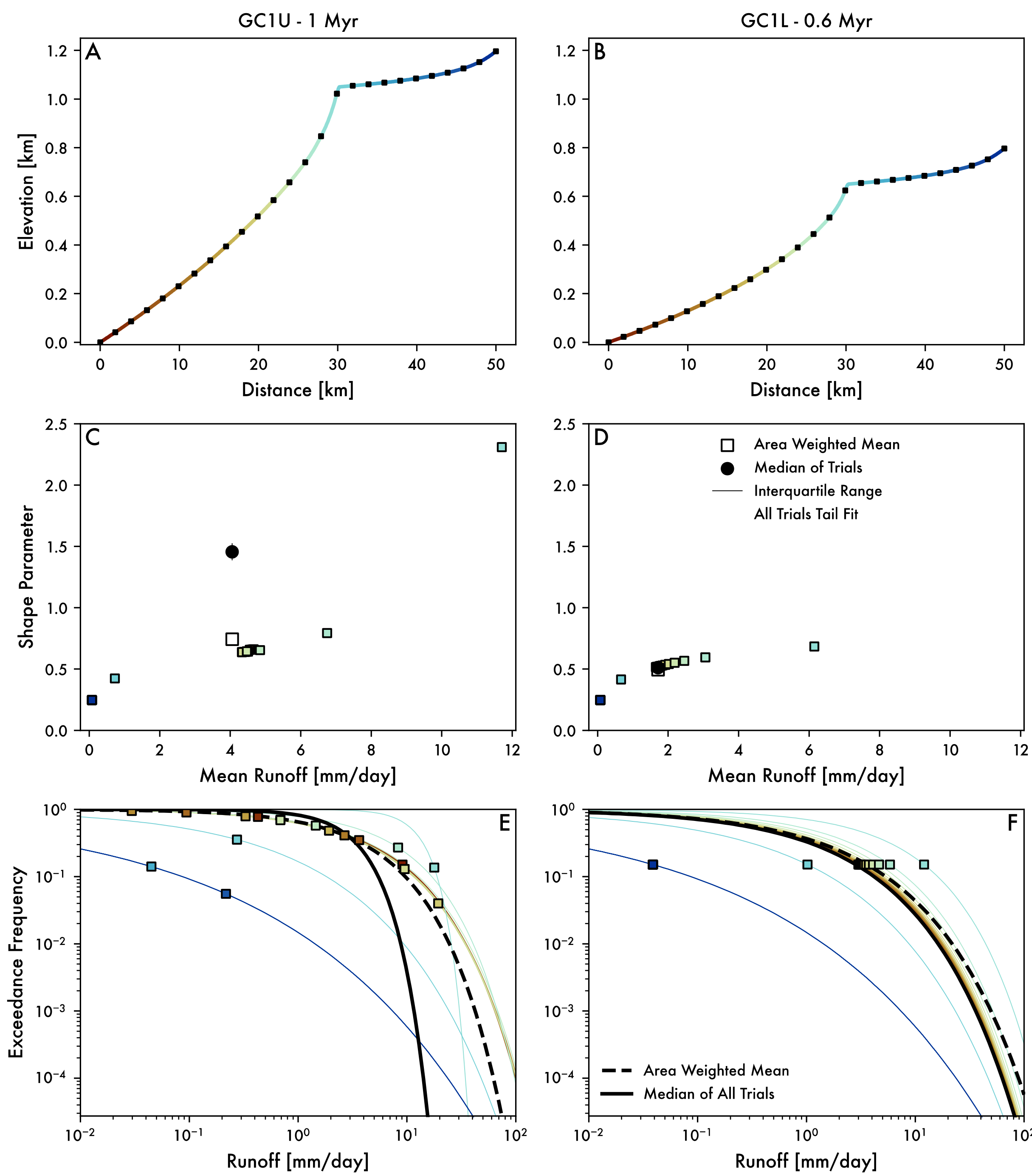

Figure 3. A) Long profile of model GC1U at 1 Myr into the model run, colors indicate individual bins and black squares mark bin boundaries. B) Same as A but for model GC1L at 0.6 Myr into the model run, which represents approximately the same point in the transient response. C) Mean runoff and variability for GC1U at 1 Myr. Colored squares are mean runoff and variability for the individual bins. White square is runoff and variability from a drainage area weighted mean of the bins. The black circle is the median of 500 trials of mean runoff and variability from routing 100 years of discharge for each trial, small gray dots are mean runoff

and variability for individual trials. D) Same a C but for model GC1L at 0.6 Myr. E) Exceedance frequency plot for GC1U at 1 Myr, showing the relationship for individual bins in the thin colored lines, the area weighted mean runoff and variability in the black dashed line, and the mean runoff and variability from the median of the 500 trials. The colored square represents runoff (and the corresponding probability of that runoff occurring) in individual bins on a random day. F) Same as E but for model GC1L at 0.6 Myr.

As described in section 3, we use both global (Figure 2A) and regional relationships (Figure 2B-C) to define the mean runoff and shape parameter within each bin. For a given time step and bin, the chain of action is: (1) Use the channel steepness from the previous step to calculate local relief using the linear relationships developed from SRTM-90 (e.g., Figure S1); (2) Use the local relief to calculate mean runoff using the power law relationships developed from WaterGAP3 (Figure 2B); (3) Also use the local relief to determine the maximum elevation by adding it to the minimum elevation within the bin; (4) Use the maximum elevation to calculate the snowmelt fraction using the power law relationships developed from WaterGAP3 (Figure 2C); and finally (5) Use the snowmelt fraction to choose the applicable global empirical relationship between mean runoff and shape parameter (Figure 2A). In this way, the mean runoff and shape parameter are updated from channel topography alone and follow data driven rules.

To ensure that the model does not extrapolate into an unreasonable part of parameter space, we impose a maximum relief that any bin can achieve. We set this to 2500 m for most runs based on a conservative estimate of what is observed in modern landscapes (e.g., Figure S1), but we also test the sensitivity of the model results to this choice (see Section 5.4). The imposition of a maximum relief is broadly consistent with the idea that there are limits to local relief set by hillslope strength (e.g., Montgomery & Brandon, 2002; Schmidt & Montgomery, 1995). Embedded in the assumption of a maximum local relief is an expectation that this should be controlled by processes not considered in our model (e.g., non-linear hillslope diffusion or mass wasting). While we do not impose a limit on maximum elevation, it has an implicit limit set by the local relief maximum. We also make sure that the snowmelt fraction cannot exceed 1 by enforcing this as an upper bound. After meeting all these constraints, each bin has a scale and shape parameter describing the probability distribution of runoffs expected for each bin at a given time step (e.g., Figure 3). To simulate the stochasticity implied by these derived parameters, we use the *SciPy weibull_min* and appropriate sub-functions to randomly extract a runoff magnitude from the relevant pdf for that bin. In detail, every 100 years of model run time, the model generates a 100 year daily time series (i.e., 36,500 days) of runoffs within each bin. This is done for efficiency as random selection of numbers from a distribution is one of the more computationally time intensive steps, but the compute time required to generate one random number is comparable to generating a large quantity of random numbers from a given distribution. This approach means that the mean runoff and variability are only updated every 100 years, but even at the maximum 8 mm/yr rock uplift rate we impose, the amount of profile change - and thus change in either relief or maximum elevation - in 100 years is sufficiently small as to not significantly influence the results. As the model evolves, at each 100 year increment when runoff time series are generated from the pdfs, the current total iteration number is used as the starting seed for the random number generator ensuring that the random numbers (i.e., runoff magnitudes) change through the model run. For each day, runoff within each bin is routed along the profile to calculate fluvial incision.

4.2. Linked versus Unlinked Cases

Whether neighboring bins are correlated or independent in time depends on how runoff events are generated in the landscape. The spatially correlated case mimics scenarios where storms or snowmelt events vary in runoff generation in space but occur contemporaneously. The spatially independent case mimics scenarios where storms or snowmelt events have systematic statistical properties with elevation, but who are independent of each other. We refer to the former as spatially 'linked' and the latter as 'unlinked'. We specifically consider these two endmember scenarios by simulating the probability of exceedance of runoff magnitudes that occur within the bins on a given day as (1) completely independent (Figure 3E) or (2) the same across all bins (Figure 3F). Implementation of the unlinked vs linked scenarios is set by changing the pseudorandom seed number. For linked scenarios, the seed for the 100-year time series is set by the iteration number for all bins. In contrast, for the unlinked case, the seed *i* is incremented by 1, such that for bin 1, the seed is *i*, for bin 2, the seed is *i+1*, and so on. It is important to note that for the unlinked case, the size of the bins represents an assumed characteristic scale of runoff events. Real landscapes likely experience a mixture of small footprint, convective events and large footprint, synoptic-scale events that obscure a single representative. As highlighted by the analysis of event sizes in WaterGAP3 data from Forte & Rossi (In Review), generally smaller events are more common than larger events. We anticipate that mixtures of event sizes, like those suggested by the WaterGAP3 data, will produce intermediate behaviors and response times, which is why we consider both 'linked' and 'unlinked' scenarios for all parameter sets. We return to the importance of whether landscapes are better represented by an unlinked versus linked scenarios in the discussion.

4.3 Model parameterization

Our main objectives in this study are to extend the 1D stochastic-threshold incision model (STIM) of Lague et al. (2005) to include spatially varying daily runoff variability (spatial-STIM) and to see how coupling expected orographic patterns in runoff variability alters predictions in the steady state and transient evolution of river longitudinal profiles using stream power. It is beyond the scope of this effort to do a full sensitivity analysis on all the STIM parameters, which have already been explored in great depth (DiBiase & Whipple, 2011; Lague, 2014; Lague et al., 2005). Instead, we focus on driving our new model using empirical relationships for how mean runoff and daily runoff variability vary as a function of local relief and then test the sensitivity of our results to the differences in model structure we have added to spatial-STIM. As such, most STIM parameters (like thresholds, rock erodibilities, width scaling) are fixed in our model runs, typically to values that were calibrated to our prior work in the Greater Caucasus (Forte et al., 2022). The values of fixed parameters used in spatial-STIM are reported in Table S1. Table S2 summarizes all the parameters we do vary in our numerical experiments. The parameters we do vary are intended to answer two questions: (1) What do orographic relationships between mean runoff and daily runoff variability entail for STIM-based predictions for the relationship between channel steepness and uplift rates; and (2) How sensitive are spatial-STIM results to the new elements of model structure?

We report our river incision modeling results in two parts that reflect the two questions posed above. The first part provides results for a series of baseline cases that use a similar model structure (50-km long rivers, 2-km wide bins), albeit for both the linked and unlinked scenarios. These baseline cases represent how a ~488 km^2 area catchment responds to range of uplift rates

(0.25 to 8 mm/yr) under approximations of the modern hydroclimatic conditions of the mountainous regions of the Greater Caucasus, European Alps, and British Columbia. The second part tests the sensitivity of our findings to differences in model structure, specifically to profile length, bin size, bin number, and maximum local relief. To do this, we use the linked Greater Caucasus baseline case at rock uplift rates of 1 mm/yr as the starting point for sensitivity analyses. Sensitivity experiments vary: (1) stream length and number of bins using model setups of 10, 20, 30, 40, 50 and 100 km width bins fixed at 2 km wide, (2) maximum relief within a bin using model setups of 1500, 2000 and 2500 m, and (3) bin size using model setups of 2, 5, and 10 km wide bins. Because profile length and bin size together define the number of bins, we also run a sensitivity experiment designed to: (4) test the notion that number of bins, and thereby the granularity of how we represent the hydroclimate, is controlling the steady state k_{sn}. This latter test compares two profile lengths of 10 and 50 km long using both 5 and 10 bins.

5 Results

5.1 Model behavior for regional cases

Direct comparison of the three regional cases for a given uplift rate, profile length, and bin size provides important insights into the behavior of spatial-STIM. Figure 4 shows the temporal evolution of all three sites for both linked and unlinked runoff parameters, a bin size of 2 km, a river length of 50 km, and an uplift rate of 1 mm/yr. These time series highlight two complementary results: (1) Differences in the relief evolution of river profiles due to different hydroclimatic forcings are relatively modest at this rock uplift rate; (2) Whether the spatial parameters are linked or unlinked is much more significant, whereby unlinked scenarios nearly double both mean k_{sn} and elevation as the long profile approaches steady state (Figure 4A-B). The other panels in Figure 4 show that the temporal evolution of the erosional response (Figure 4C), mean discharge at the outlet (Figure 4D), discharge variability (Figure 4E), and maximum snow fraction (4F) exhibit a much broader range of responses depending on the site-specific rules. However, the relative insensitivity of steady state topography to different hydroclimatic rulesets as compared to the assumption of spatial correlation of runoff events suggests the need for deeper probing. While we do not intend to dismiss the importance of the different hydroclimatic rulesets here (see discussion in section 6), we focus our initial findings on model behavior on the assumption of linked versus unlinked runoff events.

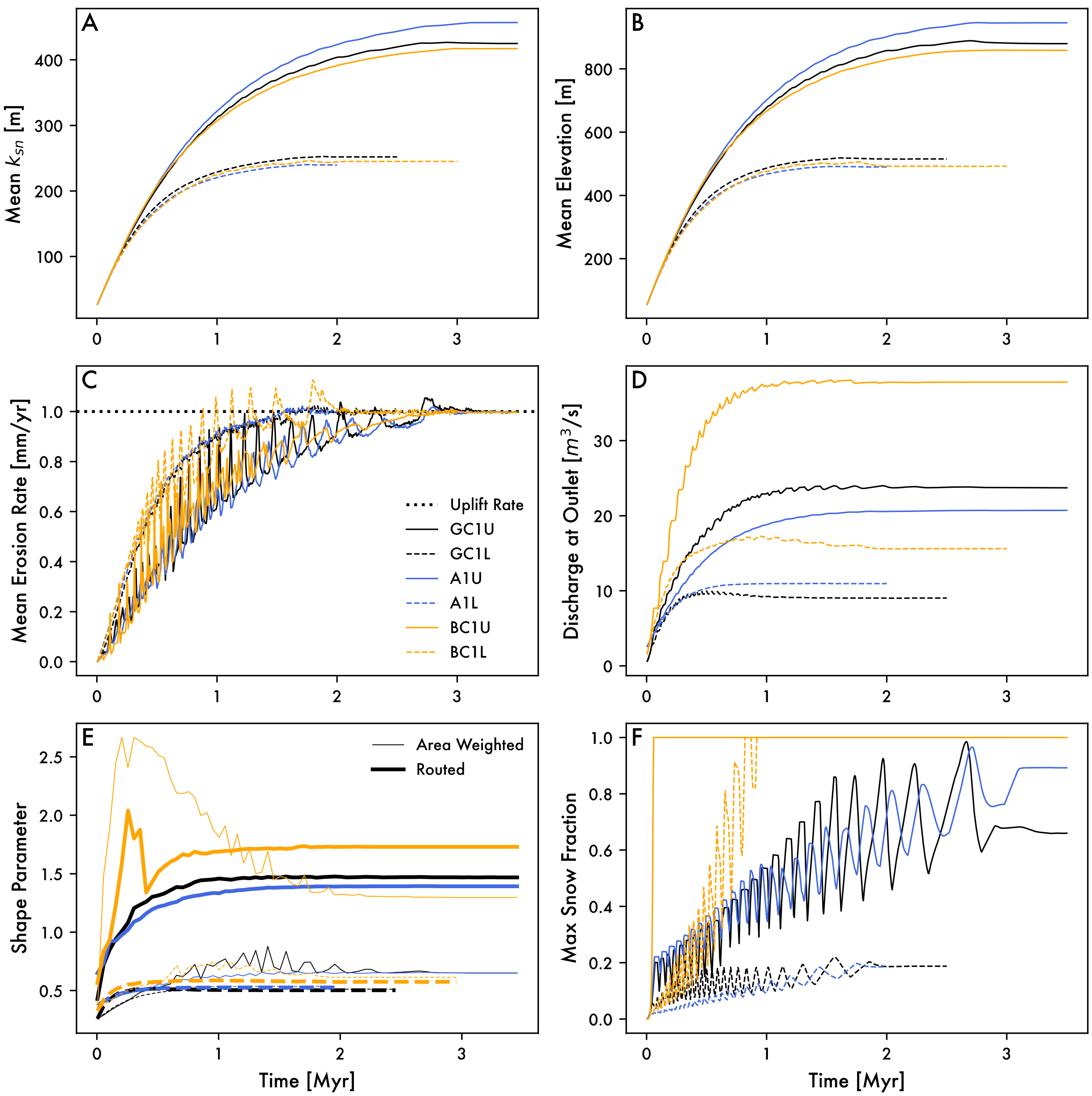

Figure 4. Evolution of 1 mm/yr models for all three locations and for both unlinked and linked cases. A) Mean k_{sn} along the profile. B) Mean elevation of the profile. C) Mean erosion rate along the profile. D) Discharge at the outlet. E) Variability of runoff at the outlet, comparing estimations from simple drainage area weighted average (thin lines) that result from routing 500 years of randomly sampled runoff for each timestep (thick lines). F) Maximum snowmelt fraction of runoff.

As the longitudinal profile evolves towards steady state, a transient slope-break knickpoint migrates upstream to accommodate the rock uplift forcing (e.g., Figure 3), much like other stream-power based models of river incision (e.g., Crosby & Whipple, 2006; Rosenbloom & Anderson, 1994). However, a key novelty to our model is that mean runoff and the shape parameter of the runoff distribution vary both in space and in time. For example, Figure 5 shows how runoff parameters vary with position during the transient case using the Greater Caucasus hydroclimatic rules. For both the unlinked and linked cases, we identified a time when the knickpoint had obtained a similar relative upstream position (Figure 3A-B; 1 Ma for unlinked; 0.6 Ma for linked). Figures 3C-F show the runoff parameters for every bin in the profile at that time. On these plots we show the spatially averaged value for the shape parameter and mean runoff. We also show the median values of these parameters for a Monte Carlo simulation (500 trials) using differently randomly sampled, 100 years long discharge records using the rulesets for this timestep. A persistent feature of unlinked cases is that the variability of routed discharge is significantly lower (i.e., larger shape parameter) than the corresponding averages of bins would suggest (Figure 3C & 3E). In linked cases, routed variability tends to be near the averages of all bins (Figure 3D & 3F). In contrast, both unlinked and linked scenarios show that mean runoff is effectively the same whether averaging across bins or from routing runoff down the profile. Regardless, the large differences between the steady state and transient behavior between unlinked and linked cases requires a closer examination of model dynamics.

An important nuanced detail of the model evolution is the extent to which during individual model runs, the range of mean runoffs and shape parameter stay within reasonable values. Specifically, while our working model (Figure 1B) envisions periods of time or locations in snowmelt dominated regimes - i.e., where there is a linear relation between mean runoff and shape parameter - that exhibit both a high magnitude of mean runoff (e.g., $\bar{R}$ > 5 mm/day) and very low variability (e.g., c_R > 1.5), the empirical data from WaterGAP3 suggests that such conditions are unlikely (Figure 2A). Considering the mean runoffs and shape parameters for each bin across the full range of uplifts and all timesteps for the Greater Caucasus unlinked model runs, as an example, highlights that the majority of bins stay within ranges observed in the empirical data without any formal restriction to this range (Figure S2).

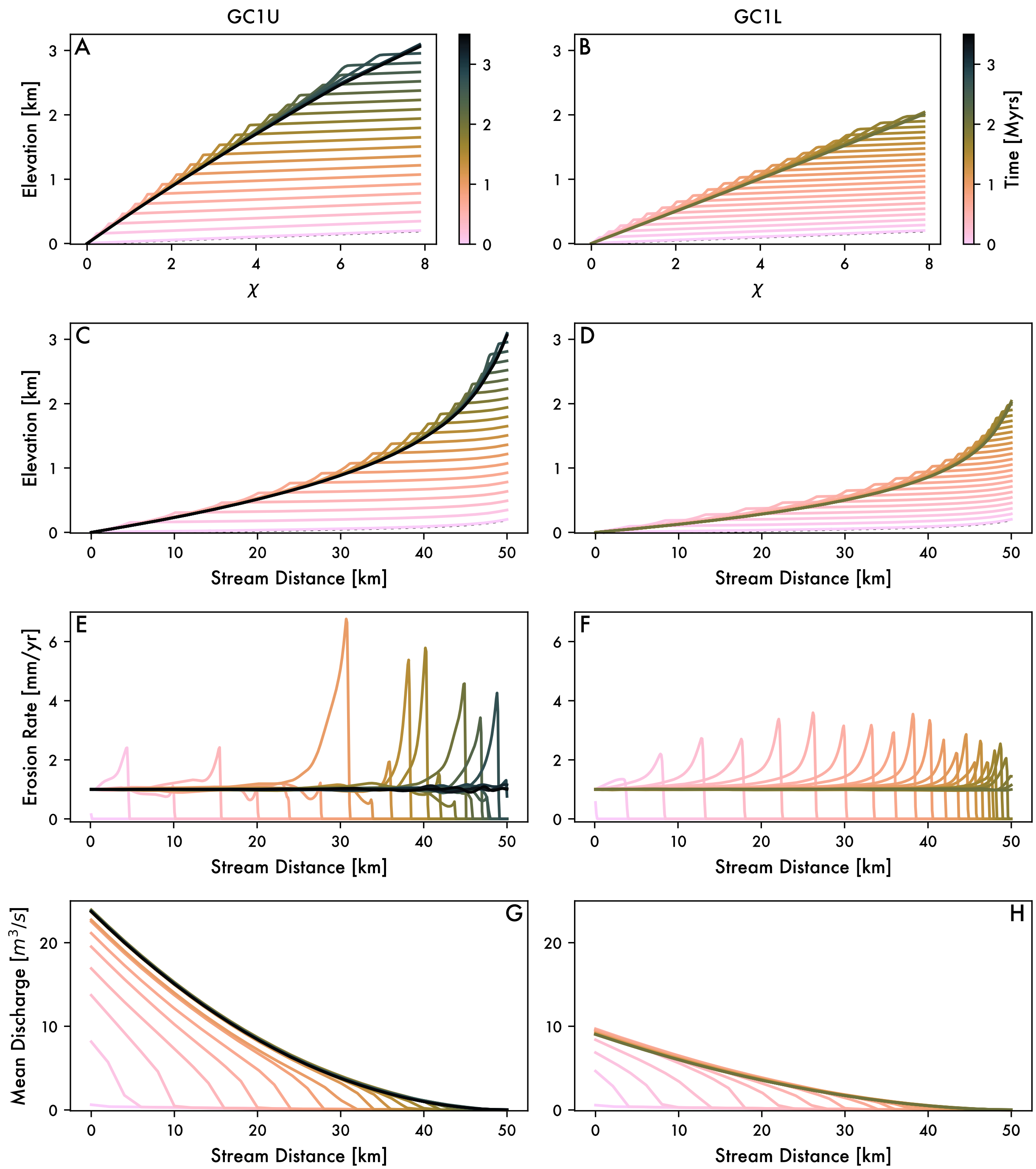

574

575 **Figure 5.** Representative stream profile evolution for an unlinked vs linked model. A) χ-
576 elevation for model GC1U through time. B) Same as A but for GC1L. C) Stream profile for
577 model GC1U through time. D) Same as C but for GC1L. E) Average erosion rate between
578 outputs along the profile for model GC1U. F) Same as E but for GC1L. G) Discharge along
579 profile for model GC1U. H) Same as G but for model GC1L.

580

5.3 Explaining differences between unlinked versus linked scenarios

To examine why there is such a large contrast between the linked and unlinked cases, Figure 5 shows contrasts between the linked and unlinked scenarios as a function of χ and stream distance for the Greater Caucasus hydroclimatic parameters. The temporal evolution of χ-elevation plots (Figure 5A-B) and longitudinal profiles (Figure 5C-D) reiterate that unlinking the runoff parameters as a function of location reduces the overall efficiency of erosion. While erosional efficiency is going down, the unlinked hydroclimatic parameters actually produce more significant pulses in erosion rate during the transient evolution of the profile (Figure 5E-F) and greater mean discharges (Figure 5G-H). Unlinked cases also generally take longer to reach steady state (Figure 5). We briefly offer our explanation for these results.

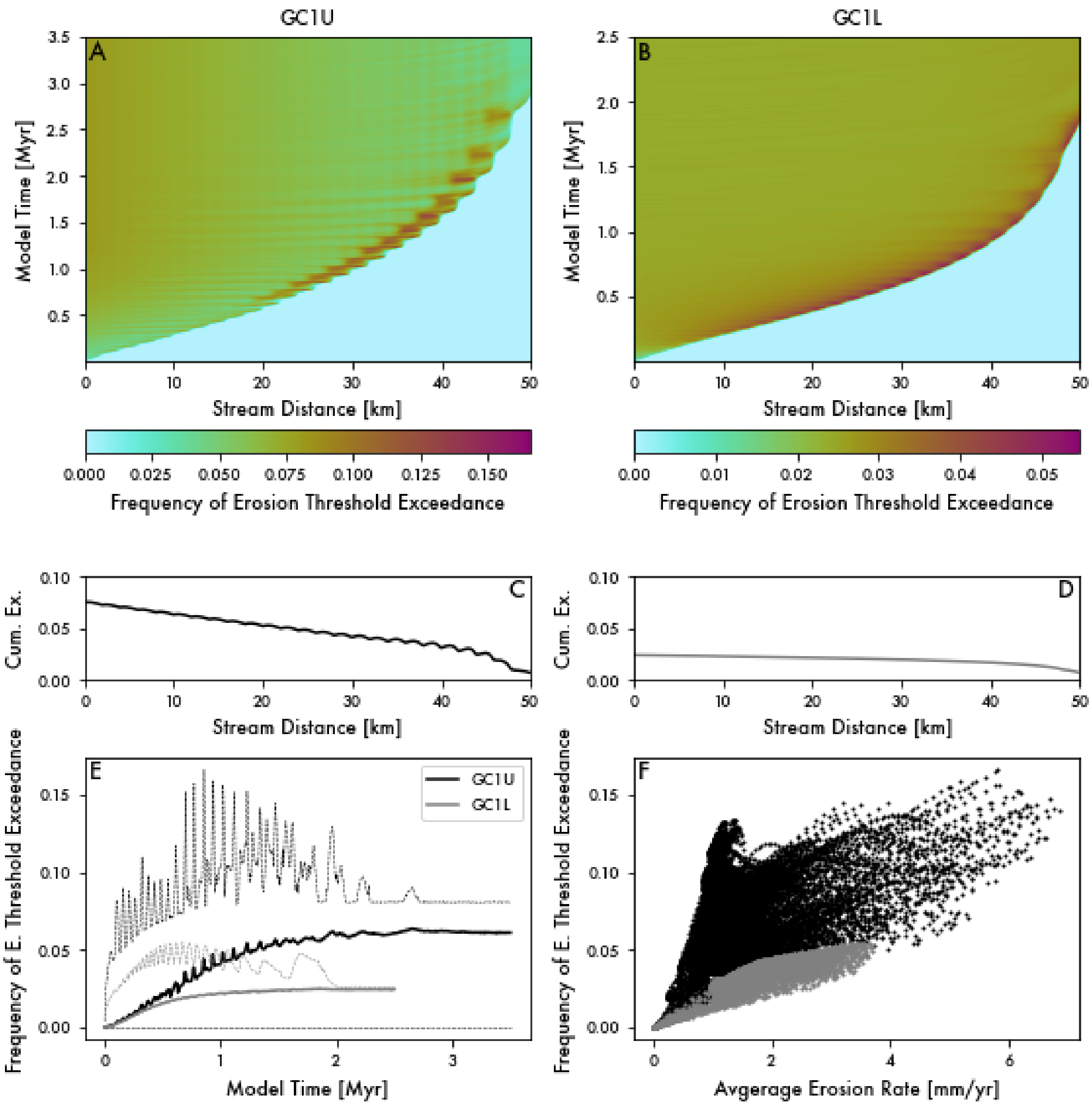

Figure 6. Frequency of exceedance of the erosion threshold between output timesteps in an unlinked vs linked scenario. A) Plot of frequency of exceedance as a function of profile distance (x) and model time (y) for the unlinked GC1U model, the area of consistently higher frequency of exceedance tracks the movement of the knickpoint through the profile. B) Same as A but for the linked GC1L model, notice that the color scale changes between A and B to highlight structure in both models. C) Cumulative frequency of exceedance of the erosion threshold across the entire model run as a function of stream distance for unlinked model GC1U. D) Same as C but for linked model GC1L. E) Mean (solid lines) and max and minimum (dashed lines) frequency of erosion threshold exceedance through time for the GC1U and GC1L models. F) Individual frequency of exceedance of erosion threshold at a specific node compared to the average erosion rate of that note for all time steps.

Interpreting the dynamics in spatial-STIM inevitably requires understanding the frequency of exceedance of erosional thresholds in the model (Figure 6), which are fixed to one value in all of our model runs. For both the linked and unlinked scenarios, areas above the knickpoint rarely exceed the threshold for erosion and are thus passively uplifted until the knickpoint passes. The knickpoint itself focuses threshold exceedances to the area just below where channels are steepest (red areas along profile in Figure 6A-B). This hotspot in threshold exceedance is localized near the knickpoint for the unlinked case and persists in downstream reaches for the linked case. Because the knickpoint is migrating upstream, cumulative threshold exceedances as a function of stream position are relatively smooth when averaged over the long-term (Figure 6C-D) with an average that stabilizes to a single value (Figure 6E). Threshold exceedance frequencies are generally higher in the unlinked case (Figure 6F) and, locally, erosion rates can get much higher in the unlinked case (note the color scale difference between Figure 6A and 6B). Such observations alone might suggest a more efficient hydroclimate in the unlinked case. However, these river profiles are approaching steady state. Our findings argue that the river profiles need to adjust to more frequent temporal exceedances to overcome the spatial heterogeneity in runoff generation. Specifically, the unlinked case makes it much less probable that upstream reaches 'benefit' from water flowing from upstream. Higher probabilities of exceedance are needed in upstream reaches to balance rock uplift, which are accommodated by steepening, because rare runoff events are not contemporaneous. These dynamics result in a negative upstream trend in cumulative exceedance (Figure 6C) that is not observed in the linked case (Figure 6D). Taken as a whole, the linked scenarios is able to maintain lower relief at lower mean discharges because of the spatial autocorrelation of events in a river basin. This outcome, a direct result of the assumptions we use in how runoff accumulates downstream, is larger than the topographic adjustments induced by the details of the orographic rules for hydroclimate we use.

5.4 Sensitivity of spatial-STIM to other elements of model structure

While the most significant difference between model outcomes is tied to whether the runoff distributions are linked or unlinked along the river profile, other structural elements of the model are also important to model dynamics. Specifically, we interrogate how the three new model parameters added to spatial-STIM (bin size, maximum local relief, profile length) and one derived parameter (number of bins) influence model behavior (Figure 7). This latter parameter encodes the ratio between the size of the system (profile length) and the scale over which changes in hydroclimatic parameters are represented (bin size), thus embedding modification to the number of degrees of freedom that model entails.

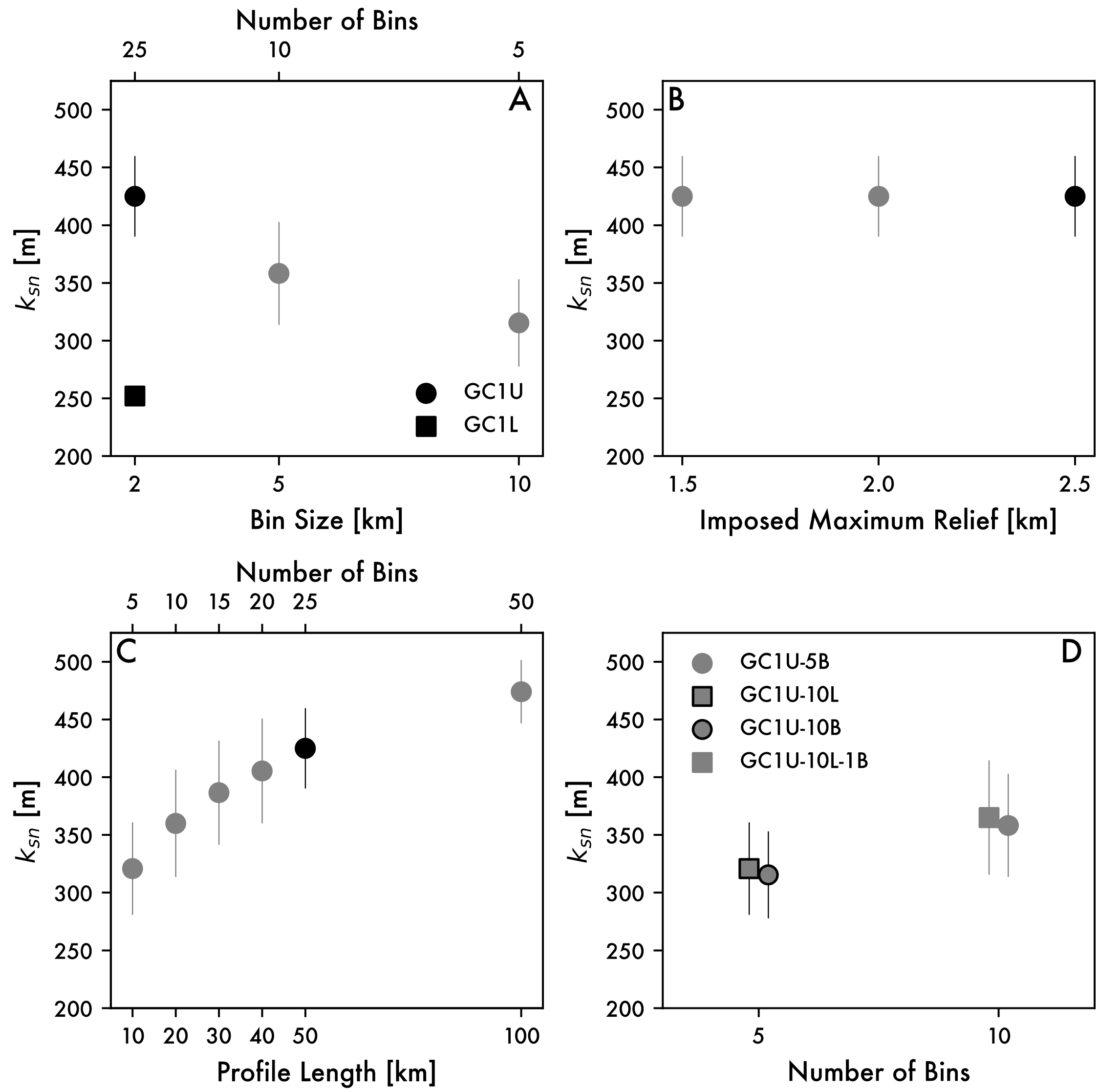

Figure 7. Summary of sensitivity experiments. Black symbols indicate results of reference experiments used elsewhere, gray symbols indicate results of a specific sensitivity experiment. Across all of the models, uplift rate is 1 mm/yr and the Greater Caucasus empirical model parameters are used. A) Effect of runoff bin size. See Figure S4 for temporal evolution of the relevant models. B) Effect of imposed maximum relief. See Figure S5 for temporal evolution of the relevant models. C) Effect of profile length. See Figure S6 for temporal evolution of the relevant models. Note that for all of these models, the bin size is kept at 2 km, so different profile lengths imply different number of bins. D) Effect of number of bins, comparing models that are either 50 km (squares - GC1U-5B, GC1U-10B) or 10 km (circles - GC1U-10L, GC1U-10L-1B) long.

For all sensitivity experiments, we use the Greater Caucasus hydroclimatic parameters and rock uplift rates of 1 mm/yr, with the steady-state channel steepness as the model target. Baseline conditions (black symbols) assume 50-km river lengths, bin sizes of 2 km, and maximum imposed relief of 2.5 km. For unlinked scenarios, the sensitivity of k_{sn} to bin size is substantial (Figure 7A, S3). A 5X increase in bin size corresponds to ~33% reduction in k_{sn}. Increasing the size of bins both decreases the granularity with which orographic gradients in hydroclimatic parameters are represented as well as increase the degree of spatial autocorrelation. To this latter point, we plotted the linked case to show that the effect of increasing bin size is approaching the k_{sn} values observed when the events are linked over the entire river profile. The sensitivity of k_{sn} to maximum local relief is near zero (Figure 7B, S4). We placed a threshold in maximum local relief to prevent extrapolating our runoff parameter relationships to unrealistic values. As such, we wanted to make sure that this threshold was not strongly influencing the long-term behavior of the model. The insensitivity of channel steepness to this maximum local relief gives us confidence our model interpretations are not unduly sensitive to this threshold parameter, though we hypothesize that if this maximum relief was set unrealistically low or high, that this would begin to influence model results. For unlinked scenarios, the sensitivity of k_{sn} to profile length, and thus system scale, is substantial (Figure 7C, S5). A 10X increase in profile length corresponds to ~50% increase in k_{sn}. Increasing the length of profiles, while holding bin size constant, increases the granularity with which orographic gradients in hydroclimatic parameters are represented by creating more bins for a given elevation gradient. Because both bin size and profile length impact the granularity of orographic gradients in runoff parameters, we also did a test where we changed the length of the profiles (10- and 50-km) for different bin numbers (Figure 7D). Systems of different lengths had similar values for k_{sn} as long the number of bins was the same. More bins, and thus finer resolving power of gradients in runoff parameters, led to slight increases in steady k_{sn}. For example, a 2X increase in bin number led to ~15% increase in k_{sn}, albeit within uncertainty of estimated values.

6 Discussion

Adding complexity to geomorphic transport laws like stream power is useful to the degree that new models are able to: (1) Be implemented over the spatiotemporal scales of interest; (2) Capture dynamics that cannot otherwise be simulated; and (3) Improve the ability to calibrate models and test hypotheses with empirical data. Given that stream power is one of the most widely used erosion laws in landscape evolution studies, we critically evaluate both the strengths and limits of adding spatiotemporal stochasticity to stream power.

6.1 Spatial-STIM and its predecessors

One useful lens through which to consider our new model results is in how spatial-STIM predictions compare to other 1D models built on stream power (Howard, 1994; Whipple & Tucker, 1999). We focus on three important metrics to evaluate how our new model compares to its predecessors—namely the steady state channel steepness, the steady state concavity, and the response time to steady states.

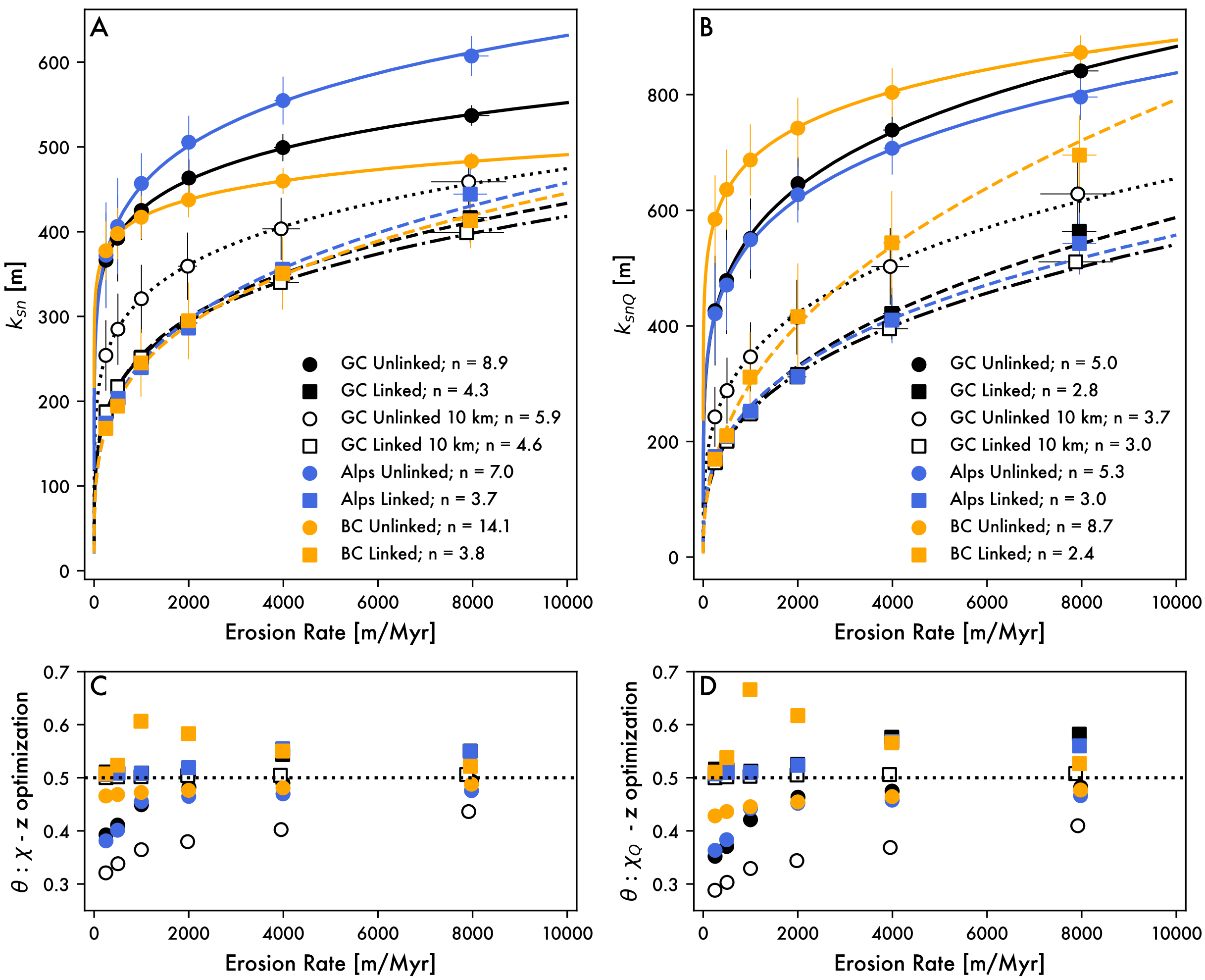

Figure 8. A) Mean k_{sn} and erosion rate at the end of each run for runs spanning erosion rates. Lines are power law fits to model results in a stream power context. Equivalent 'n' values for each stream power relationship are shown in the explanation. B) Same as A but calculating k_{snQ} sensu Adams et al., (2020). Note, for the calculation of k_{snQ} presented here, we follow Adams et al., (2020), which uses precipitation as a proxy for runoff to calculate discharge. To accomplish this in our 1D model results (which do not formally calculate precipitation), we use empirical relationships between runoff and precipitation from WaterGAP3 for each region to estimate precipitation from the modelled runoff. We compare the results of calculating k_{snQ} directly from runoff in Figure S6, but ultimately the differences are subtle. C) Best fit concavity (θ) for models using drainage area. D) Best fit concavity for models using precipitation weighted drainage area sensu Leonard et al., (2023).

6.1.1 Steady state channel steepness

Given this broader context, Figure 8 shows the steady state relationships between channel steepness and erosion rates for our regional cases using both linked and unlinked parameters. We plot results both in terms of k_{sn} and k_{snQ} using a reference channel concavity of 0.5 (see section 6.1.2 for discussion on patterns in concavity). For any given scenario, all model results are well approximated by a power law, similar to predictions from simple stream power (e.g., Equation

8). In general though, power law fits of channel steepness show strongly sublinear behavior, and imply stream power values of *n* of ~3.5 – 4.5 for linked scenarios and ~6 – 14 for unlinked scenarios (Figure 8A). That individual scenarios imply different values for *K* and *n* should be expected because these stream power parameters encode details of both climate and rock properties (e.g., Kirby & Whipple, 2012; Whipple et al., 2022), the former of which we are explicitly varying in the different scenarios. However, the wide range and large magnitudes of *n* are a bit more surprising and could be interpreted as local channel steepness thresholds (Hilley et al., 2019). Consistent with other stochastic-threshold models of river incision (see Lague, 2014 for discussion), effective values of *n* are positively correlated with the shape parameter of the runoff distribution (Figure 9A), though our results are not entirely analogous. The relationship between the shape parameter of the runoff distribution and *n* largely emerges from the unlinked cases in our model results. For linked cases, which are more similar to the Lague et al. (2005) model, similar runoff variabilities produce a wide range of values for *n*. Furthermore, a negative correlation between *K* and mean runoff emerges from the spatially varying hydroclimatic rules used to evolve the profiles (Figure 9C).

While we do not perform a formal "ground truthing" of our model results, we can consider comparisons between measured and modeled k_{sn}-*E* relationships from the Greater Caucasus (Figure S7), where the underlying STIM parameters (e.g., k_e, τ_c, k_w) are approximately calibrated based on Forte et al., (2022). Comparisons of the simple SPIM type fits to different sets of linked vs unlinked, basin size, and corresponding number of bins suggests that such a "random sampling" across basins with different underlying stochastic parameters is an acceptable explanation for the array of erosion rates observed there (e.g., Figure S7).

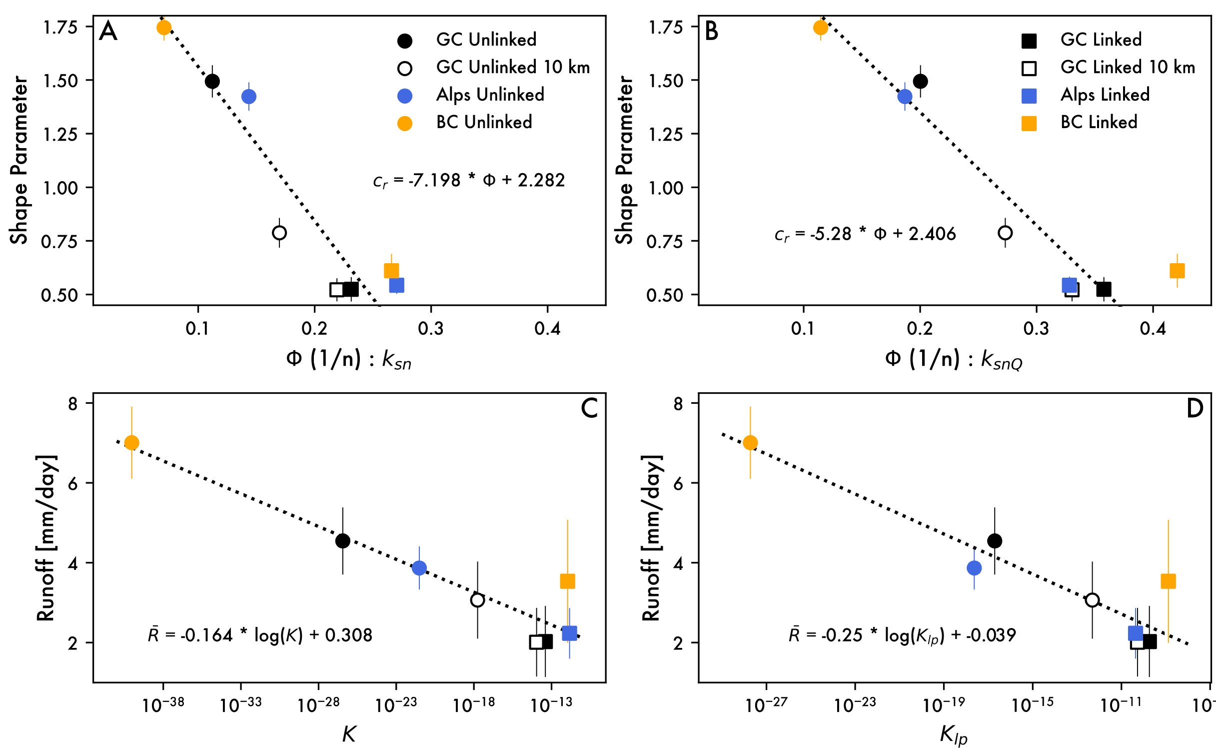

Figure 9. A) Mean shape parameter across models for a given scenario compared to 1/n from fits in 8A. B) Mean variability across models for a given scenario compared to 1/n from fits in 8B. C) Mean runoff across models for a given scenario compared to K from fits in 8A. D) Mean runoff across models for a given scenario compared to K_{lp} from fit in 8B.

We also present the similar topography erosion rate relationships using an alternative calculation of channel steepness. We do this to explore whether normalizing our calculations by spatial gradients in runoff can help collapse model results onto a single relationship, thus following up on the recent empirical successes of using k_{snQ} (Adams et al., 2020; Leonard et al., 2023). Using k_{snQ} instead of k_{sn} does reduce the overall range of stream power values of n to ~2.4 - 3 for linked cases and ~5 – 8.7 for unlinked cases (Figure 8B). However, this modified form of channel steepness does not significantly collapse the data onto a single relationship, as might otherwise be expected for model runs with the same underlying 'rock properties' (i.e., same values for k_e, τ_c, and k_w). The point is emphasized further in the persistence of trends between shape parameter and n (Figure 9B) and runoff and K_{lp} (Figure 9D) for values from the k_{snQ}-E relationships (Figure 8B). The overall relationships between stream power parameters and the two different calculations of channel steepness are quite similar, though they differ in detail as the rank order of values between k_{sn} (Figure 9A; 9C) and k_{snQ} (Figure 9B; 9D) are different.

6.1.2 Steady state concavity

One possible explanation for the complex suite of relationships between channel steepness and erosion rates shown in Figure 8A-B is that our model scenarios produce systematic variations in concavity. Other 1D river incision models show that steady state concavity is differentially sensitive to orographic gradients in precipitation as a function of rock uplift rate (Roe et al., 2003), though they typically fall within the range of expected values between 0.4 and 0.6 (Whipple et al., 2022). As such, we consider best-fit concavities both using drainage area (Figure 8C) and precipitation-weighted drainage area (Figure 8D). For each model run, we determine the best-fit concavity by using the linear relationship between χ-elevation or χ_Q-elevation (sensu Leonard et al., 2023). Given that all model runs use a ratio of the area exponent, m, to the slope exponent, n, of 0.5, deviations from this value indicate concavity anomalies induced by differences in how runoff is generated in the model. The range of concavities is relatively large, spanning from ~0.3 to 0.6. Importantly, unlinked scenarios consistently develop profiles with concavities < 0.5. In contrast, linked scenarios consistently develop profiles with concavities > 0.5. While the largest anomalies (i.e., positive and negative deviations from 0.5) often occur at lower uplift rates, though this is not universally true. For example, the British Columbia hydroclimatic parameters produce concavities that are relatively insensitive to rock uplift rates when bins are unlinked, but display strong, non-monotonic sensitivity when the bins are linked (Figure 8C-D). Because there is a tradeoff between the relative roles of mean runoff and daily runoff variability on erodibility, numerical models like spatial-STIM are needed to identify how sensitive concavity is to rock uplift rates. For a given set of hydroclimatic parameters, concavity can vary by ~0.1. We also note that precipitation-weighted concavity (Figure 8D) shows more sensitivity to rock uplift rates than conventional calculations of concavity. This is the opposite of the effect described in Leonard et al. (2023), where these authors showed that precipitation-weighted concavity reduces the dynamic range of values observed in central Andean drainages. Based on this, we suggest that systematic changes in channel concavity with rock uplift rates may provide important insights into the importance of orographic effects on runoff parameters and the relative scale of runoff generating events, e.g., synoptic events may be more analogous to linked cases and convective events may be more analogous to unlinked cases.

6.1.3 Transient response timescales

Stream power predictions of steady state morphology are non-unique (Gasparini & Brandon, 2011). By instead targeting the functional relationship between channel steepness and erosion rate for a given set of environmental conditions (e.g., rock properties, climatic setting), stream power predictions are more discriminating, but are still non-unique. For example, there is always a K and n - or K_{lp} and n - pair that describes the expected steady state topography produced by our model outputs for each of the simulated scenarios (Figures 8-9). As such, we consider here whether differences in model dynamics are observed in the transient behavior of the 1D river profiles. To assess this, we compared the response times to steady state for both spatial-STIM and simple stream power. We calculated the analytical solution to stream power using the equations in Whipple (2001). Using the Hack parameters from model initialization (Eq. 21), we can derive the analytical solution for response time using the fit values for K and n for each model scenario. To do this, we first back-calculate the initial rock uplift rates that correspond to the initial k_{sn} of 25 m used in all model runs. We then calculate the fractional change in rock uplift rates and apply the equations in Whipple (2001) to calculate a response time. For comparison to spatial-STIM, we have to also define steady state in our numerical runs. We define the time to steady state as the time it takes for the absolute value of the difference between maximum elevations of the profiles to fall below 0.1 m. Figure 10 summarizes these calculations and includes direct comparison between spatial-STIM and the analytical solutions for stream power (Figure 10C). Response times for spatial-STIM plot very close to the 1:1 line, suggesting broad agreement. Importantly, while it is clear that the simple stream power model can reproduce the transient dynamics of spatial-STIM, the values of K and n cannot be derived from first principles. In other words, the values for these parameters are not readily inferred from known differences in modern estimates of mean runoff and daily runoff variability of our three regional cases. This is further emphasized in comparisons of modeled vs observed k_{sn}-E relationships for the Greater Caucasus (e.g., Figure S7).

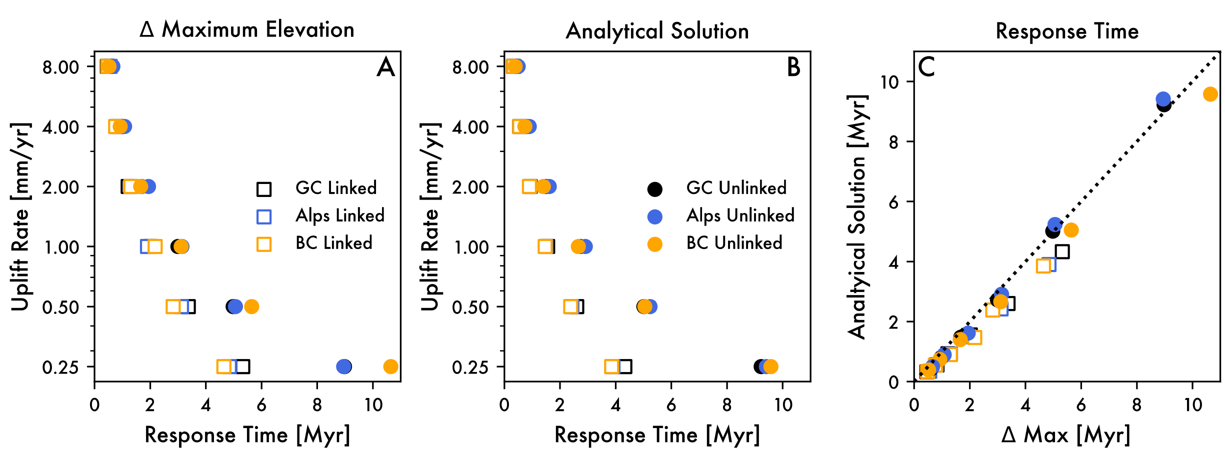

Figure 10. Comparison of analytical steady state (SPIM) to empirical steady state (STIM). A) Estimated time to steady-state from model initiation using the change in maximum elevation between saved timesteps and defining steady-state as when the absolute value of this metric

drops below 0.1 m. B) Analytical solution for response time using estimates of K and n from Figure 8 and calculating what the effective initial uplift rate for each model was assuming this K and n and the starting k_{sn} (25 m) to calculate the appropriate fractional change in uplift rate sensu Whipple (Whipple, 2001). C) Comparison of the empirical and analytical response times.

6.1.4 Utility of spatial-STIM

The stream power approximation for each scenario simulated in this study adequately explains both the steady state and transient response of river profiles. However, there are other reasons to favor spatial-STIM. Any attempt to calibrate a 1D model of river incision is going to attempt to constrain free parameters using observational data. While most of our model parameters are fixed, we were able to produce a very wide range of behaviors in spatial-STIM by simply including empirical patterns between mean runoff and runoff variability at the three regional sites. Surprisingly, the details of our hydroclimatic rules were less important than one new structural element of our model (i.e., linking or unlinking bins) that handles the spatial autocorrelation of runoff events. As an illustrative example, consider that we have good evidence for 'mixed' populations of runoff generating events being sourced from snowmelt and rainfall-runoff in the Greater Caucasus (Forte et al., 2022). Using the same set of hydroclimatic rules, the K and n for linked and unlinked cases are very different. Attempting to fit a stream power relationship to an arbitrary mix of these two cases would likely produce hybrid values of K and n that are not reflective of either runoff source or the expected behavior of the system, e.g., response time or the extrapolation of channel steepness to estimates of erosion rates.

Our model analysis also shows that unlinked models were quite sensitive to the characteristic scales of runoff events (Figure 7A) and watershed size (Figure 7C). These findings place central importance on understanding the climatic controls on the ratio of these two spatial scales (Figure 7D) if we want to understand the topographic response to base level fall. Empirical studies (e.g., Binnie et al., 2007; Cyr et al., 2010; DiBiase et al., 2010; Forte et al., 2022; Harkins et al., 2007; Miller et al., 2013; Olivetti et al., 2012; Ouimet et al., 2009; Rossi et al., 2017; Safran et al., 2005; Scherler et al., 2014) typically sample across a range of watershed sizes that may be interacting in complex ways with the characteristic scale of runoff generating events that may themselves vary with landscape position and contributions from snowmelt (Forte & Rossi, In Review). Given this strong sensitivity to spatial scale, it is unclear how generalizable empirical estimates of K and n are when comparing across landscapes. While typical uncertainties associated with erosion thresholds (e.g., Shobe et al., 2018), rock erodibility (e.g., Yanites et al., 2017), channel width scaling (e.g., Gallen & Fernández-Blanco, 2021), and sediment flux dynamics (e.g., Whipple & Tucker, 2002) still remain (and were not explored in this analysis), we argue from our simulations that we may not be accounting even for the most important aspects of climate in current models of bedrock river incision.

6.2 Implications on climate-tectonic coupling

We undertook this analysis to understand how orographic gradients in mean runoff and daily runoff variability alter predictions for the topographic evolution of mountain ranges as they grow (e.g., Figure 1). Specifically, we focused on the important transition from rainfall-dominated probability distributions to snowmelt-dominated ones as topography grows, based on our own findings in the Greater Caucasus (Forte et al., 2022). Analysis of WaterGAP3 model data revealed that these hydrological transitions may be generally important to mid-latitude mountain ranges where glacial erosion is still limited (Forte & Rossi, In Review). Our new 1D model of river incision shows that if such orographic gradients are honored, then it is relatively easy to generate highly sub-linear ($3 < n < 14$) relationships between channel steepness and erosion rates that might otherwise be interpreted as mechanistically ambiguous channel steepness thresholds (Hilley et al., 2019). While the snowmelt transition was our target, the model behavior we show in this analysis is more general. As long as there is an inverse relationship between mean runoff and daily runoff variability (e.g., Molnar et al., 2006; Rossi et al., 2016) and mean runoff increases as topography (i.e., relief) grows, then the dynamics of our model simulations will apply. Assuming a constant set of hydroclimatic variables as mountain ranges grow is likely unrealistic, and thus we argue that increasingly sublinear relationships between topography and erosion may be the norm and not the exception. Early hypotheses on climate-tectonic feedbacks assumed that the most important orographic effects are in extracting precipitation on the windward side and diminishing precipitation on the leeward size of topographic barriers (e.g., Beaumont et al., 1992; Whipple & Meade, 2006; Willett, 1999). Subsequent efforts focused on the importance of mountain topography setting the spatial distribution of precipitation (Roe et al., 2003) and phase of precipitation in mountain landscapes (Anders et al., 2008). While all these orographic effects are undoubtedly important, our model simulations provide a natural progression to these insights by also accounting for how stochastic runoff generation (DiBiase & Whipple, 2011; Lague et al., 2005; Tucker, 2004) will itself be a function of the relief evolution of mountain ranges. Our results further highlight that a critical, and largely ignored, set of parameters associated with the scale of runoff events with respect to watershed size may be fundamental to understanding potential feedbacks between climate and tectonics.

6.3 Limitations and Future Directions

While our new model provides important insights into how realistic orographic gradients in runoff generation will impact stream-power based predictions for topographic relief, there are several important limitations to our model analysis to keep in mind. First, we only use modern relationships between local relief and mean runoff, maximum elevation, snowmelt fraction at select locations to drive model scenarios. Related to this assumption is that the observed relationships will persist across geologically long periods of time, even though we know that mean precipitation varies with broader climate cyclicity and glacial-interglacial forcing (e.g., Cruz et al., 2005; Wang et al., 2008). As such, we would expect that both mean runoff, runoff variability, and snowmelt fraction should all vary, perhaps significantly, across glacial-interglacial cycles or larger climate transitions. One novelty of our model is that it makes explicit the rules that describe how hydroclimatology will coevolves with topographic relief. To take advantage of this model feature in simulating glacial-interglacial cycles, we need more detailed accounting for how these cycles impact mean runoff and daily runoff variability through time. Second, the discrete boundaries imposed by binning the river profile is quite imperfect. Not only does it imply a scale beyond which runoff parameters can be treated independently, it also fixes the location of these event properties in space. The arbitrary locations of these bins are likely an unrealistically hard constraint on the event-scale properties of snowmelt and rainfall-runoff events.

Keeping these limitations in mind, we highlight a few promising directions for future modeling and data analysis on this topic. As computational power increases, we are seeing more realistic simulations of orographic precipitation in bedrock river incision modeling (e.g., Han et al., 2015; Shen et al., 2021). Our results suggest that these efforts would benefit from bringing commensurate improvement in the land surface models that convert precipitation to runoff. For mid-latitude mountain landscapes, it is important to honor the importance of precipitation phase on orographic gradients in runoff patterns (e.g., Anders et al., 2008; Forte et al., 2022; Rossi et al., 2020). Similarly, prior studies highlight the potential importance of Milankovitch forcings on precipitation for landscape evolution (Godard et al., 2013). How these cyclical variations of precipitation are then converted to mean runoff, daily runoff variability, and snowmelt fraction is thus an important unknown. Our focus on the form of k_{sn}-E relationships suggest that a natural extension of this work should also be to examine how spatial-STIM might alter coupled models between climate and tectonics. Relatively simple analytical approaches to this problem (Whipple & Meade, 2004, 2006), as well as more complex dynamical models (e.g., Braun & Yamato, 2010; Roe et al., 2006; Stolar et al., 2007), have yielded important insights into potential feedbacks between climate and tectonics. While we can say that the dynamics in our 1D model will act to dampen such feedbacks, the question of by how much is still open and deserves more careful study.

Finally, the assumption of spatial autocorrelation of runoff events proved to be the strongest regulator of erosional efficiency in our new model structure. Within the context of a 1D models like ours, having events that are stochastic in space and time is challenging, but not insurmountable. As such, we need more hydrological studies that can help us generalize the spatial statistics of rainfall- and snowmelt-runoff events. Promising work characterizing potentially significant spatial variability in precipitation patterns in high relief landscapes exist (e.g., Anders et al., 2006, 2007; Barros et al., 2000; Campbell & Steenburgh, 2014; Frei & Schär, 1998; Minder et al., 2008), but generalizing these into how this spatial stochasticity is, or is not, reflected in runoff at a similar scale remains largely unclear. Similarly, the analysis of WaterGAP3 data by Forte & Rossi (In Review) suggested a fundamental relationship between runoff event size and contribution from snowmelt with events with larger footprints being dominated by high proportions of snowmelt, further highlighting the interconnectedness of many of the parameters we consider. While fully distributed hydrological models come at a high computational cost for landscape evolution studies, statistical descriptions of these dynamics may be tractable over landscape evolution timescales. Furthermore, the way space is represented in 1D river profiles may not be able to fully mimic the spatial statistics of runoff events, thereby requiring 2D landscape evolution modeling. The Landlab modeling library (Barnhart et al., 2020; Hobley et al., 2017) already has many of the process components suited to implementing spatial-STIM in a 2D framework. Thus understanding how well we have captured spatiotemporal stochasticity using the assumptions of our 1D model is an important open question that should be tested in 2D (Tucker, 2004; Tucker & Bras, 2000). Despite the clear needs for refining and understanding the applicability of spatial-STIM, our findings show that simply accounting for spatial variations in daily runoff variability is an important step towards generating testable predictions for the erosion laws used by our community.

7 Conclusions

Results from simulations using our new empirically driven 1D profile model that considers both temporal and spatial stochasticity in runoff and snowmelt events highlight that generally sublinear relationships between channel steepness and erosion rate are an expected outcome of orographic development within mountain ranges. Specifically that because of the linkage between mean runoff and runoff variability wherein increasing mean runoff drives decreasing variability, development of orographic gradients in runoff imply orographic gradients in runoff variability. This is strengthened by the tendency for increasing elevation of mountain ranges to preferentially accumulate snow, driving a greater component of runoff to be related to snowmelt and further reducing the variability of runoff. Given the expectation that decreasing runoff variability should lead to increasingly sublinear channel steepness erosion rate relationships, this implies a potential negative feedback between the topographic growth of mountain range and continued steepening and provides a process based explanation for the observation of pseudo-thresholds in channel steepness erosion rate relationships.

A critical outcome of our model results is also that a fundamental parameter for controlling the nature of channel steepness erosion rate relationships is the extent to which the probability of exceedance of runoff events within a given catchment are "linked" or "unlinked" and the corresponding spatial scale of individual runoff events in cases where these probabilities are unlinked. These two endmember states roughly correspond to the extent to which runoff generating events in a given catchment tend to be dominated by spatially restricted convective storm events or more spatially broad synoptic events. Broadly, for identical parameters, unlinked scenarios predict steeper landscapes than the equivalent linked scenario. This implies a fundamental scale dependence on the nature of channel steepness erosion rate relationships and an expectation that smaller catchments would be more dominated by synoptic events or convective storm events that are the same size or larger than the catchment (i.e., linked) whereas larger catchments are more likely to be sensitive to spatially restricted runoff generating events (i.e., unlinked), but this can be importantly modified by local weather and storm patterns. In the context of the majority of empirical channel steepness erosion rate relationships from catchment averaged cosmogenic nuclides, we would broadly expect that many such datasets from a single mountain range reflect mixtures of catchments that could either best be described as linked or unlinked scenarios. While for a single set of hydroclimatological parameters and assuming a linked or unlinked scenario, the resulting channel steepness erosion rate pattern can be fit by a simple stream power relationship, the extent to which this is meaningful in real datasets, where linked and unlinked type catchments are mixed, is unclear. Ultimately, our results have important implications not only for our understanding of expected coupling between hydroclimatology, topography, and tectonics as a mountain range grows, but also the type of observations we as a community should be considering within our datasets. Future work should focus on both considering the implications of spatial and temporal stochasticity of runoff and snowmelt events within 2D, but also better empirical quantification of the characteristic spatial and temporal scale of runoff events within mountainous catchments and how these evolve with time through glacial-interglacial cycles.

Acknowledgments

Support for M.W. Rossi came from the Geomorphology and Land-use Dynamics (GLD) Program (EAR-1822062). Neither AMF or MWR have any real or perceived financial or other conflicts with the contents of this work.

Open Research

Analysis and model codes necessary to reproduce this work are housed in the GitHub repository (https://github.com/amforte/snowmelt_orography) with stable release doi: 10.5281/zenodo.8115140. All model results, additional figures summarizing the results of each model run, and larger outputs of the processing steps are available through the Zenodo repository doi:10.5281/zenodo.7665887. Portions of these analysis codes rely on publicly available datasets that we do not have permission to redistribute, but when used, we provide comments in the code referencing where these datasets can be downloaded.

References

Adams, B. A., Whipple, K. X., Forte, A. M., Heimsath, A. M., & Hodges, K. V. (2020). Climate controls on erosion in tectonically active landscapes. *Science Advances*, *6*(42). https://doi.org/10.1126/sciadv.aaz3166

Alcamo, J., Döll, P., Henrichs, T., Kaspar, F., Lehner, B., Rösch, T., & Siebert, S. (2003). Development and testing of the WaterGAP 2 global model of water use and availability. *Hydrological Sciences Journal*, *48*(3), 317–337. https://doi.org/10.1623/hysj.48.3.317.45290

Anders, A. M., Roe, G. H., Hallet, B., Montgomery, D. R., Finnegan, N. J., & Putkonen, J. (2006). Spatial patterns of precipitation and topography in the Himalaya. In S. D. Willett, N. Hovius, M. T. Brandon, & D. M. Fisher, *Tectonics, Climate, and Landscape Evolution*. Geological Society of America. https://doi.org/10.1130/2006.2398(03)

Anders, A. M., Roe, G. H., Durran, D. R., & Minder, J. R. (2007). Small-Scale Spatial Gradients in Climatological Precipitation on the Olympic Peninsula. *Journal of Hydrometeorology*, *8*(5), 1068–1081. https://doi.org/10.1175/JHM610.1

Anders, A. M., Roe, G. H., Montgomery, D. R., & Hallet, B. (2008). Influence of precipitation phase on the form of mountain ranges. *Geology*, *36*(6), 479. https://doi.org/10.1130/G24821A.1

Barnhart, K. R., Hutton, E. W. H., Tucker, G. E., Gasparini, N. M., Istanbulluoglu, E., Hobley, D. E. J., et al. (2020). Short communication: Landlab v2.0: a software package for Earth surface dynamics. *Earth Surface Dynamics*, *8*(2), 379–397. https://doi.org/10.5194/esurf-8-379-2020

Barros, A. P., Joshi, M., Putkonen, J., & Burbank, D. W. (2000). A study of the 1999 monsoon rainfall in a mountainous region in central Nepal using TRMM products and rain gauge observations. *Geophysical Research Letters*, *27*(22), 3683–3686. https://doi.org/10.1029/2000GL011827

Beaumont, C., Fullsack, P., & Hamilton, J. (1992). Erosional control of active compressional orogens. In K. R. McClay (Ed.), *Thrust Tectonics* (pp. 1–18). New York: Chapman Hall.

Berghuijs, W. R., Woods, R. A., Hutton, C. J., & Sivapalan, M. (2016). Dominant flood generating mechanisms across the United States: Flood Mechanisms Across the U.S. *Geophysical Research Letters*, *43*(9), 4382–4390. https://doi.org/10.1002/2016GL068070

Binnie, S. A., Phillips, W. M., Summerfield, M. A., & Fifield, L. K. (2007). Tectonic uplift, threshold hillslopes, and denudation rates in a developing mountain range. *Geology*, *35*(8), 743–746. https://doi.org/10.1130/G23641A.1

Bookhagen, B., & Burbank, D. (2006). Topography, relief, and TRMM-derived rainfall variations along the Himalaya. *Geophysical Research Letters*, *33*, L08405–L08405. https://doi.org/10.1029/2006GL026037

Bookhagen, B., & Burbank, D. (2010). Toward a complete Himalayan hydrological budget: Spatiotemporal distribution of snowmelt and rainfall and their impact on river discharge. *Journal of Geophysical Research*, *115*(F03019). https://doi.org/10.01029/02009JF001426

Bookhagen, B., & Strecker, M. R. (2008). Orographic barriers, high-resolution TRMM rainfall, and relief variations in the eastern Andes. *Geophysical Research Letters*, *35*(L06403). https://doi.org/10.1029/2007GL032011

Braun, J., & Yamato, P. (2010). Structural evolution of a three-dimensional, finite-width crustal wedge. *Tectonophysics*, *484*, 181–192.

Campbell, L. S., & Steenburgh, W. J. (2014). Finescale Orographic Precipitation Variability and Gap-Filling Radar Potential in Little Cottonwood Canyon, Utah. *Weather and Forecasting*, *29*(4), 912–935. https://doi.org/10.1175/WAF-D-13-00129.1

Campforts, B., Vanacker, V., Herman, F., Vanmaercke, M., Schwanghart, W., Tenorio, G. E., et al. (2020). Parameterization of river incision models requires accounting for environmental heterogeneity: insights from the tropical Andes. *Earth Surface Dynamics*, *8*(2), 447–470. https://doi.org/10.5194/esurf-8-447-2020

Coulthard, T. J., & Skinner, C. J. (2016). The sensitivity of landscape evolution models to spatial and temporalrainfall resolution. *Earth Surface Dynamics*, *4*(3), 757–771. https://doi.org/10.5194/esurf-4-757-2016

Crosby, B. T., & Whipple, K. X. (2006). Knickpoint initiation and distribution within fluvial networks: 236 waterfalls in the Waipaoa River, North Island, New Zealand. *Geomorphology*, *82*, 16–38.

Cruz, F. W., Burns, S. J., Karmann, I., Sharp, W. D., Vuille, M., Cardoso, A. O., et al. (2005). Insolation-driven changes in atmospheric circulation over the past 116,000 years in subtropical Brazil. *Nature*, *434*(7029), 63–66. https://doi.org/10.1038/nature03365

Cyr, A. J., Granger, D. E., Olivetti, V., & Molin, P. (2010). Quantifying rock uplift rates using channel steepness and cosmogenic nuclide-determined erosion rates: Examples from northern and southern Italy. *Lithosphere*, *2*(3), 188–198.

Deal, E., Braun, J., & Botter, G. (2018). Understanding the Role of Rainfall and Hydrology in Determining Fluvial Erosion Efficiency. *Journal of Geophysical Research: Earth Surface*, *123*(4), 744–778. https://doi.org/10.1002/2017JF004393

Desormeaux, C., Godard, V., Lague, D., Duclaux, G., Fleury, J., Benedetti, L., et al. (2022). Investigation of stochastic-threshold incision models across a climatic and morphological gradient. *Earth Surface Dynamics*, *10*(3), 473–492. https://doi.org/10.5194/esurf-10-473-2022

DiBiase, R. A., & Whipple, K. X. (2011). The influence of erosion thresholds and runoff variability on the relationships among topography, climate, and erosion rate. *Journal of Geophysical Research*, *116*(F04036). https://doi.org/10.1029/2011JF002095

DiBiase, R. A., Whipple, K. X., Heimsath, A. M., & Ouimet, W. B. (2010). Landscape form and millennial erosion rates in the San Gabriel Mountains, CA. *Earth and Planetary Science Letters*, *289*(1–2), 134–144.

Döll, P., Kaspar, F., & Lehner, B. (2003). A global hydrological model for deriving water availability indicators: model tuning and validation. *Journal of Hydrology*, *270*(1–2), 105–134. https://doi.org/10.1016/S0022-1694(02)00283-4

Dunne, T., & Black, R. D. (1970). Partial Area Contributions to Storm Runoff in a Small New England Watershed. *Water Resources Research*, *6*(5), 1296–1311. https://doi.org/10.1029/WR006i005p01296

Farr, T. G., Rosen, P. A., Caro, E., Crippen, R., Duren, R., Hensley, S., et al. (2007). The shuttle radar topography mission. *Reviews of Geophysics*, *45*, 1–33.

Ferrier, K. L., Huppert, K. L., & Perron, J. T. (2013). Climatic control of bedrock river incision. *Nature*, *496*(7444), 206–209. https://doi.org/10.1038/nature11982

Flint, J. J. (1974). Stream gradient as a function of order, magnitude, and discharge. *Water Resources Research*, *10*, 969–973.

Forte, A. M., & Rossi, M. W. (In Review). Stochastic in space and time: Part 1, Characterizing Orographic Gradients in Mean Runoff and Daily Runoff Variability. *Journal of Geophysical Research - Earth Surface*.

Forte, A. M., & Whipple, K. X. (2019). Short communication : The Topographic Analysis Kit (TAK) for TopoToolbox. *Earth Surface Dynamics*, *7*, 87–95. https://doi.org/10.5194/esurf-7-87-2019

Forte, A. M., Whipple, K. X., Bookhagen, B., & Rossi, M. W. (2016). Decoupling of modern shortening rates, climate, and topography in the Caucasus. *Earth and Planetary Science Letters*, *449*, 282–294. https://doi.org/10.1016/j.epsl.2016.06.013

Forte, A. M., Leonard, J. S., Rossi, M. W., Whipple, K. X., Heimsath, A. M., Sukhishvili, L., et al. (2022). Low variability runoff inhibits coupling of climate, tectonics, and topography in the Greater Caucasus. *Earth and Planetary Science Letters*, *584*. https://doi.org/10.1016/j.epsl.2022.117525

Frei, C., & Schär, C. (1998). A precipitation climatology of the Alps from high-resolution rain-gauge observations. *International Journal of Climatology*, *18*(8), 873–900. https://doi.org/10.1002/(SICI)1097-0088(19980630)18:8<873::AID-JOC255>3.0.CO;2-9

Gallen, S. F., & Fernández-Blanco, D. (2021). A New Data-driven Bayesian Inversion of Fluvial Topography Clarifies the Tectonic History of the Corinth Rift and Reveals a Channel Steepness Threshold. *Journal of Geophysical Research: Earth Surface*. https://doi.org/10.1029/2020JF005651

Gasparini, N. M., & Brandon, M. T. (2011). A generalized power law approximation for fluvial incision of bedrock channels. *Journal of Geophysical Research: Earth Surface*, *116*(F2). https://doi.org/10.1029/2009JF001655

Godard, V., Tucker, G. E., Fisher, G. B., Burbank, D. W., & Bookhagen, B. (2013). Frequency-dependent landscape response to climatic forcing. *Geophysical Research Letters*, *40*, 859–863. https://doi.org/10.1002/grl.50253

Hack, J. T. (1957). *Studies of longitudinal stream profiles in Virignia and Maryland* (pp. 97–97).

Han, J., Gasparini, N. M., & Johnson, J. P. L. (2015). Measuring the imprint of orographic rainfall gradients on the morphology of steady-state numerical fluvial landscapes: OROGRAPHIC RAINFALL AND STEADY-STATE FLUVIAL LANDSCAPES. *Earth Surface Processes and Landforms*, *40*(10), 1334–1350. https://doi.org/10.1002/esp.3723

Harel, M. A., Mudd, S. M., & Attal, M. (2016). Global analysis of the stream power law parameters based on worldwide 10Be denudation rates. *Geomorphology*, *268*, 184–196. https://doi.org/10.1016/j.geomorph.2016.05.035

Harkins, N., Kirby, E., Heimsath, A. M., Robinson, R., & Reiser, U. (2007). Transient fluvial incision in the headwaters of the Yellow River, northeastern Tibet, China. *Journal of Geophysical Research*, *112*, F03S04-F03S04.

Hilley, G. E., Porder, S., Aron, F., Baden, C. W., Johnstone, S. A., Liu, F., et al. (2019). Earth's topographic relief potentially limited by an upper bound on channel steepness. *Nature Geoscience*, *12*(10), 828–832. https://doi.org/10.1038/s41561-019-0442-3

Hobley, D. E. J., Adams, J. M., Nudurupati, S. S., Hutton, E. W. H., Gasparini, N. M., Istanbulluoglu, E., & Tucker, G. E. (2017). Creative computing with Landlab: an open-source toolkit for building, coupling, and exploring two-dimensional numerical models of Earth-surface dynamics. *Earth Surface Dynamics*, *5*(1), 21–46. https://doi.org/10.5194/esurf-5-21-2017

Howard, A. D. (1994). A detachment-limited model of drainage basin evolution. *Water Resources Research*, *30*(7), 2261–2285.

Kirby, E., & Whipple, K. X. (2012). Expression of active tectonics in erosional landscapes. *Journal of Structural Geology*, *44*, 54–75.

Lague, D. (2014). The stream power river incision model: evidence, theory and beyond. *Earth Surface Processes and Landforms*, *39*(1), 38–61. https://doi.org/10.1002/esp.3462

Lague, D., Hovius, N., & Davy, P. (2005). Discharge, discharge variability, and the bedrock channel profile. *Journal of Geophysical Research*, *110*, F04006–F04006. https://doi.org/10.1029/2004JF000259

Lehner, B., Verdin, K., & Jarvis, A. (2008). New Global Hydrography Derived From Spaceborne Elevation Data. *Eos, Transactions American Geophysical Union*, *89*(10), 93. https://doi.org/10.1029/2008EO100001

Leonard, J. S., Whipple, K. X., & Heimsath, A. M. (2023). Isolating climatic, tectonic, and lithologic controls on mountain landscape evolution. *Science Advances*, *9*(3), eadd8915. https://doi.org/10.1126/sciadv.add8915

Marder, E., & Gallen, S. F. (2023). Climate control on the relationship between erosion rate and fluvial topography. *Geology*. https://doi.org/10.1130/G50832.1

Miller, S. R., Sak, P. B., Kirby, E., & Bierman, P. R. (2013). Neogene rejuvination of central Appalachian topography: Evidence for differential rock uplift from stream profiles and erosion rates. *Earth and Planetary Science Letters*, *369*, 1–12.

Minder, J. R., Durran, D. R., Roe, G. H., & Anders, A. M. (2008). The climatology of small-scale orographic precipitation over the Olympic Mountains: Patterns and processes. *Quarterly Journal of the Royal Meteorological Society*, *134*(633), 817–839. https://doi.org/10.1002/qj.258

Molnar, P., Anderson, R. S., Kier, G., & Rose, J. (2006). Relationships among probability distributions of stream discharges in floods, climate, bed load transport, and river incision. *Journal of Geophysical Research*, *111*, F02001–F02001. https://doi.org/10.1029/2005JF000310

Montgomery, D. R., & Brandon, M. T. (2002). Topographic controls on erosion rates in tectonically active mountain ranges. *Earth and Planetary Science Letters*, *201*, 481–489.

Olivetti, V., Cyr, A. J., Molin, P., Faccenna, C., & Granger, D. E. (2012). Uplift history of the Sila Massif, southern Italy, deciphered from cosmogenic Be-10 erosion rates and river longitudinal profile analysis. *Tectonics*, *31*, TC3007–TC3007. https://doi.org/10.1029/2011TC003037

Ouimet, W. B., Whipple, K. X., & Granger, D. E. (2009). Beyond threshold hillslopes: Channel adjustment to base-level fall in tectonically active mountain ranges. *Geology*, *37*(7), 579–582.

Peleg, N., Skinner, C., Ramirez, J. A., & Molnar, P. (2021). Rainfall spatial-heterogeneity accelerates landscape evolution processes. *Geomorphology*, *390*, 107863. https://doi.org/10.1016/j.geomorph.2021.107863

Perron, J. T., & Royden, L. H. (2013). An integral approach to bedrock river profile analysis. *Earth Surface Processes and Landforms*, *38*, 570–576. https://doi.org/10.1002/esp.3302

Pitlick, J. (1994). Relation between peak flows, precipitation, and physiography for five mountain regions in the western USA. *Journal of Hydrology*, *158*, 219–240.

Roe, G. H. (2005). OROGRAPHIC PRECIPITATION. *Annual Review of Earth and Planetary Sciences*, *33*(1), 645–671. https://doi.org/10.1146/annurev.earth.33.092203.122541

Roe, G. H., Montgomery, D. R., & Hallet, B. (2002). Effects of orographic precipitation variations on the concavity of steady-state river profiles. *Geology*, *30*(2), 143–146.

Roe, G. H., Montgomery, D. R., & Hallet, B. (2003). Orographic precipitation and the relief of mountain ranges. *Journal of Geophysical Research*, *108*(B6). https://doi.org/10.1029/2001JB001521

Roe, G. H., Stolar, D. B., & Willett, S. D. (2006). Response of a steady-state critical wedge orogen to changes in climate and tectonic forcing. In S. D. Willett, N. Hovius, M. T. Brandon, & D. Fisher (Eds.), *Tectonics, climate, and landscape evolution* (Vols. 1–398, pp. 239–272).

Rosenbloom, N., & Anderson, R. S. (1994). Hillslope and channel evolution in a marine terraced landscape, Santa Cruz, California. *Journal of Geophysical Research*, *99*(B7), 14013–14029.

Rossi, M. W., Whipple, K. X., & Vivoni, E. R. (2016). Precipitation and evapotranspiration controls on event-scale runoff variability in the contiguous United States and Puerto Rico. *Journal of Geophysical Research*, *121*. https://doi.org/10.1002/2015JF003446

Rossi, M. W., Quigley, M. C., Fletcher, J. M., Whipple, K. X., Díaz-torres, J. J., Seiler, C., et al. (2017). Along-strike variation in catchment morphology and cosmogenic denudation rates reveal the pattern and history of footwall uplift , Main Gulf Escarpment , Baja California. *Geological Society of America Bulletin*. https://doi.org/10.1130/B31373.1

Rossi, M. W., Anderson, R. S., Anderson, S. P., & Tucker, G. E. (2020). Orographic Controls on Subdaily Rainfall Statistics and Flood Frequency in the Colorado Front Range, USA. *Geophysical Research Letters*, *47*(4). https://doi.org/10.1029/2019GL085086

Safran, E. B., Bierman, P. R., Aalto, R., Dunne, T., Whipple, K. X., & Caffee, M. W. (2005). Erosion rates driven by channel network incision in the Bolivian Andes. *Earth Surface Processes and Landforms*, *30*, 1007–1024.

Sassolas-Serrayet, T., Cattin, R., & Ferry, M. (2018). The shape of watersheds. *Nature Communications*, *9*(1), 1–8. https://doi.org/10.1038/s41467-018-06210-4

Scherler, D., Bookhagen, B., & Strecker, M. R. (2014). Tectonic control on 10 Be-derived erosion rates in the Garhwal. *Journal of Geophysical Research: Earth Surface*, *119*(August 2013), 83–105. https://doi.org/10.1002/2013JF002955

Scherler, D., DiBiase, R. A., Fisher, G. B., & Avouac, J.-P. (2017). Testing monsoonal controls on bedrock river incision in the Himalaya and Eastern Tibet with a stochastic-threshold stream power model. *Journal of Geophysical Research: Earth Surface*, *122*, 1389–1429. https://doi.org/10.1002/2016JF004011

Schmidt, K. M., & Montgomery, D. R. (1995). Limits to relief. *Science*, *270*(5236), 617–620.

Schwanghart, W., & Scherler, D. (2014). Short Communication: TopoToolbox 2 - MATLAB based software for topographic analysis and modeling in Earth surface sciences. *Earth Surface Dynamics*, *2*, 1–7. https://doi.org/10.5194/esurf-2-1-2014

Shen, H., Lynch, B., Poulsen, C. J., & Yanites, B. J. (2021). A modeling framework (WRF-Landlab) for simulating orogen-scale climate-erosion coupling. *Computers & Geosciences*, *146*, 104625. https://doi.org/10.1016/j.cageo.2020.104625

Shobe, C. M., Tucker, G. E., & Rossi, M. W. (2018). Variable-Threshold Behavior in Rivers Arising From Hillslope-Derived Blocks. *Journal of Geophysical Research: Earth Surface*, *123*(8), 1931–1957. https://doi.org/10.1029/2017JF004575

Snyder, N. P., Whipple, K. X., Tucker, G. E., & Merrits, D. J. (2003). Importance of a stochastic distribution of floods and erosion thresholds in the bedrock river incision problem. *Journal of Geophysical Research*, *108*(B2). https://doi.org/10.1029/2001JB001655

Stolar, D. B., Roe, G. H., & Willett, S. D. (2007). Controls on the patterns of topography and erosion rate in a critical orogen. *Journal of Geophysical Research*, *112*(F04002). https://doi.org/10.1029/2006JF000713

Tucker, G. E. (2004). Drainage basin sensitivity to tectonic and climatic forcing: Implications of a stochastic model for the role of entrainment and erosion thresholds. *Earth Surface Processes and Landforms*, *29*, 185–204. https://doi.org/10.1002/esp.1020

Tucker, G. E., & Bras, R. L. (2000). A stochastic approach to modeling the role of rainfall variability in drainage basin evolution. *Water Resources Research*, *36*(7), 1953–1964.

Wang, Y., Cheng, H., Edwards, R. L., Kong, X., Shao, X., Chen, S., et al. (2008). Millennial- and orbital-scale changes in the East Asian monsoon over the past 224,000 years. *Nature*, *451*(7182), 1090–1093. https://doi.org/10.1038/nature06692

Whipple, K. X. (2001). Fluvial landscape response time: How plausible is steady-state denudation? *American Journal of Science*, *301*, 313–325.

Whipple, K. X. (2009). The influence of climate on the tectonic evolution of mountain belts. *Nature Geoscience*, *2*, 97–104.

Whipple, K. X., & Meade, B. (2004). Controls on the strength of coupling among climate, erosion, and deformation in two-sided, frictional orogenic wedges at steady state. *Journal of Geophysical Research*, *109*, F01011–F01011. https://doi.org/10.1029/2003JF000019

Whipple, K. X., & Meade, B. (2006). Orogen response to changes in climatic and tectonic forcing. *Earth and Planetary Science Letters*, *243*, 218–228.

Whipple, K. X., & Tucker, G. E. (1999). Dynamics of the stream-power river incision model: Implications for height limits of mountain ranges, landscape response timescales, and research needs. *Journal of Geophysical Research*, *104*(B8), 17661–17674.

Whipple, K. X., & Tucker, G. E. (2002). Implications of sediment-flux-dependent river incision models for landscape evolution. *Journal of Geophysical Research*, *107*(B2). https://doi.org/10.1029/2000JB000044

Whipple, K. X., DiBiase, R. A., Crosby, B., & Johnson, J. P. L. (2022). Bedrock Rivers. In J. (Jack) F. Shroder (Ed.), *Treatise on Geomorphology (Second Edition)* (pp. 865–903). Oxford: Academic Press. https://doi.org/10.1016/B978-0-12-818234-5.00101-2

Willett, S. D. (1999). Orogeny and orography: The effects of erosion on the structure of mountain belts. *Journal of Geophysical Research*, *104*(B12), 28,957-28,981.

Wobus, C. W., Whipple, K. X., Kirby, E., Snyder, N. P., Johnson, J., Spyropolou, K., et al. (2006). Tectonics from topography: Procedures, promise, and pitfalls. In S. D. Willett, N. Hovius, M. T. Brandon, & D. Fisher (Eds.), *Tectonics, climate, and landscape evolution* (Vols. 1–398, pp. 55–74). Boulder, CO: The Geological Society of America.

Yanites, B. J., Becker, J. K., Madritsch, H., Schnellmann, M., & Ehlers, T. A. (2017). Lithologic Effects on Landscape Response to Base Level Changes: A Modeling Study in the Context of the Eastern Jura Mountains, Switzerland. *Journal of Geophysical Research: Earth Surface*, *122*(11), 2196–2222. https://doi.org/10.1002/2016JF004101